# Analysis and Design of a Low Reynolds Propeller for Optimal Unmanned Aerial Vehicle (UAV) Flight

by

Alan Mushynski

A Report Submitted to the Faculty of the

Milwaukee School of Engineering

In Partial Fulfillment of the

Requirements for the Degree of

Master of Science in Engineering

Milwaukee, Wisconsin
May 2016

## Abstract

The purpose of this capstone project was to develop a method to optimize an airfoil and propeller for a multicopter operating in a low Reynolds number state. The capstone project is being submitted to meet the requirements for the Milwaukee School of Engineering's (MSOE) Master of Science in Engineering (MSE) program. Multicopters – also known as a multirotors -- are normally a type of Micro aerial vehicle (MAV). The multicopter features two or more rotor blades; thus, a tricopter, quadcopter, hexacopter and octocopter refer to three-, four-, six-, and eight-rotor helicopters, respectively. MAVs are subject to different fluid flows as a result of operating at low Reynolds numbers, normally less than 300,000. This lowers the efficiencies in the propellers because of the higher drag forces on the airfoils. Optimization methods have been previously explored for large-scale propellers but as these larger propellers operate at a higher Reynolds number, the airfoils would not scale to an efficient small propeller. A few optimization methods have been developed for MAVs, but these have been for traditional airplane-style aircraft that have different design requirements. This study discusses methods to model the airfoils and the modified blade element momentum theory to optimize the propeller. The airfoil optimization is conducted with a combination of a MATLAB program for airfoil geometry and the use of Xfoil to provide the airfoil flight characteristics. Xfoil is a publicly licensed interactive design and analysis software tool that was first developed at the Massachusetts Instituite of Technology (MIT). A second optimization is performed in MATLAB using the optimized airfoils to determine the best blade pitch, chord length and blade taper for a propeller for each airfoil. Two of the top designs were modeled in Solidworks and then tested with computational fluid dynamics (CFD) software (Flow Simulation) to compare with the theoretical results from MATLAB. The results from the CFD software were imported into a finite element analysis (FEA) software package (Simulation) to verify the propeller would withstand the forces applied from the motor running at its maximum output to a factor of safety (FOS) no less than 1.5. Both of the propellers tested provided the required thrust during a near hovering state, while improving efficiency over the stock propeller.

## Acknowledgments

Obtaining my Master's degree was a goal that would not have been possible without the assistance, guidance and support of many people.

I would like to especially thank my wife, Dawn Mushynski, and my children, Jessica and Aeryn, for their continued loving support through the long nights and weekends spent working on my schooling and for taking an interest in my studies.

I would like to thank TJ Johnson, for his assistance with all of my engineering endeavors and for his friendship. Without these I would not have reached the place where I am at today.

Lastly, I would like to thank the engineering department at MSOE for giving me the chance to attend the school and for all of their assistance throughout my degree program.

# Table of Contents

# List of Figures

# List of Tables

# Nomenclature

*Symbols*

a – Change in Velocity prior to Actuator of the Slipstream

A – Area of a wing

Ab - Rotor blade area

b – Change in Velocity after the Actuator of the Slipstream

b – Blade Width

B – Number of Blades in a Propeller or Tip Loss Factor

c – Chord Length

$C_d$ – Coefficient of Drag

$C_l$ – Coefficient of Lift

$C_t$ – Coefficient of Thrust

D – Drag

D – Diameter

FOM – Figure of Merit

g – Grams

H – Head Pressure

J – Geometric Advance

K – APC Propeller Constant

L – Lift

N – Number of blades for Hover Equations

P – Static Pressure

P'- Pressure Lowered by Propeller

q – Dynamic Pressure

Q – Torque

$Q_c$ – Coefficient of Torque

r – Radius

R – Tip Radius

S – Area of Blade or Airfoil

S – Solidity Factor

T – Thrust

$T_c$- Coefficient of Thrust

U – Resultant velocity at the blade element

$U_t$ – In plane velocity, parallel to rotor disk

$U_p$ – Out of plane velocity, normal to the rotor disk

V – Velocity

W – Weight

$V_a$ – Velocity change caused by actuator

$V_b$ – Velocity change caused by actuator and slipstream

$\Delta$ – Change in value

$\Phi$ – Angle between direction of motion in a blade element and the plane of rotation

$\alpha$ – Angle of attack

$\beta$ – Blade Angle

$\gamma$ – Angle between lift and resultant force of an airfoil

$\varepsilon$ – Angle of Downwash

$\eta$ – Efficiency

$\rho$ – Density of Air

$\lambda$ – Rotor inflow ratio

$\sigma$ – Rotor solidity

$\theta$ – Blade pitch angle

$\Omega$ – Rotational frequency of the rotor

$\upsilon$ – Kinematic viscosity coefficient

*Abbreviations*

BEM or BEMT– Blade Element Momentum Theory

CAD – Computer Aided Design

CFD – Computational Fluid Dynamics

FEA—Finite Element Analysis

MAV – Micro Air Vehicles

RPM – Revolutions Per Minute

UAV – Unmanned Aerial Vehicle

VTOL – Vertical Takeoff and Landing

## Introduction

Over the past five years, the industry--both civilian and government use--for small Unmanned Aerial Vehicles (UAVs) and Micro Aerial Vehicles (MAVs) has increased significantly. This growth is because of the large number of applications these devices can be easily adapted to. A few of these applications include search and rescue, wildfire observation and management, security, allowing military personnel to search areas without risk of harm to themselves, photography and hobbyist uses [1]. This large demand has driven innovation for designs to include better flight characteristics, more efficient motors, better batteries to improve flight times, and more robust controls [2, 3, 4, 5]. However, as this is still a fairly new market, there is a lot of potential for improvements in various aspects of the designs.

One design factor that has not been adequately addressed is the propeller performance. Propellers for full-sized aircraft and some large-scale models have undergone thorough design advancements and physical testing, and have been well documented for over one hundred years [6, 7, 8, 9]. The documented performance testing for large-scale propellers allows designers to choose the most efficient design for a propeller, based on which flight characteristics are desired for an aircraft. Unfortunately, these performance data do not apply well to the smaller versions of the propellers because of the change in airfoil flight characteristics [9]. The propellers used on MAV applications are normally in the range of four inches to less than twenty-four inches [10]. The use of small chord lengths and the generally low forward velocity of the MAV cause the propellers to operate at a low Reynolds number, normally less than 300,000 and as low as 50,000 to 100,000 [11, 12]. The Reynolds number has a large effect on the performance of an airfoil in relation to the

lift versus drag characteristics [13]. Figure 1 shows the maximum lift-to-drag ratio for an U.S.A 35B airfoil based on changing Reynolds numbers at a fixed angle of attack. As the Reynolds number decreases below 700,000, the lift decreases and the drag increases. This is caused by the airflow around the airfoil being in a laminar state and not separating from the airfoil to allow a turbulent wake, and this state of affairs increases the drag of the airfoil.

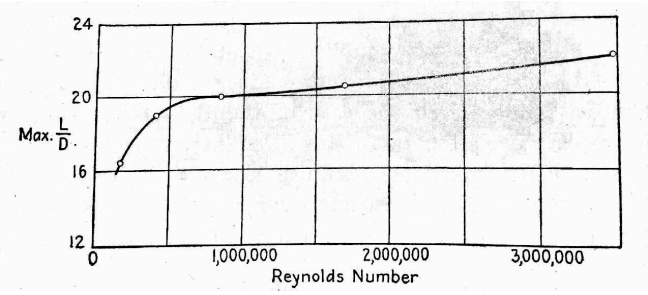


**Figure 1: U.S.A 35B Airfoil Lift to Drag Ratio for Varying Reynolds Numbers [6].**

Currently, propellers for MAVs are predominately chosen from off-the-shelf options from various companies by a trial and error approach, use of an estimation equation [14, 15], or a recommendation may be provided by the motor manufacturer [10]. Equations (1), (2), (3), and (4) -- from Boucher [14] -- show the estimation procedure:

$$Prop\ Power\ (Watts) = K * D^4 * RPM^3 Pitch, \quad (1)$$

$$K = 1.11\ for\ APC\ Type\ Propellers\ , \quad (2)$$

$$K = 1.21\ for\ APC - E\ Type\ Propellers\ , \quad (3)$$

and

$$D: Pitch = 1:1\ for\ speed\ and\ 2:1\ for\ high\ thrust. \quad (4)$$

The propeller is selected by first choosing if the speed or high thrust is more desirable for the application. Based on the style of propeller chosen, either APC or APC-E, the K constant is used with the motor wattage and maximum revolutions per minute (RPM),

and the flight characteristic for the propeller to determine the best pitch and diameter for the application.

These off-the-shelf propellers are either based on full sized version flight characteristics, but scaled down to meet the design requirements of the application, or they are based on airfoils in which neither the drawings nor the design data are normally provided to the public. As these propellers are normally untested, it is hard for a designer to choose the best propeller for the applications at hand. Wind tunnel testing has been performed on a small sample of designs to determine their propeller performance, but these tests were done without knowing the desired flight characteristics that cause a large range of efficiencies. With respect to testing done at the University of Illinois at Urbana-Champaign, the efficiencies ranged from 28% to just over 60% [12] on some off-the-shelf propellers.

The MAVs can be broken into two main categories, including aircraft that generate lift with wings and aircraft that generate lift with propellers. The aircraft that generate lift with a wing resemble either traditional airplane shapes, including single or multiple wings, or other experimental types such as those using flapping wings for flight. Aircraft that generate lift with propellers are either a helicopter or multicopter configuration. Multicopter aircraft include tricopters, quadcopters, hexcopters and multiple other configurations that are only limited by the designer's intent for the aircraft. The naming convention of the multicopter designates the number of propellers being used in the design, such as a tricopter, which consists of three propellers. The propeller efficiency is of greater importance for multicopter aircraft because they only generate lift with the propellers as they fly without the use of fixed wing, much like a helicopter. A high efficiency is harder to obtain with a multicopter because not only does the small chord length for the propeller lower the

Reynolds number and therefore increase the drag, but the forward velocity, in this case an upwards velocity, is also normally low or can be zero in hover cases. Because a multicopter has low propeller efficiency, it will be susceptible to shorter flight times, lower responsiveness during flight, and increased wear on the batteries.

The purpose of this capstone research project was to design an airfoil and propeller that are optimized for a 3Drobotics Iris+ quadcopter. The optimization was made with the primary goal of achieving the best flight characteristics for normal hovering with small movements, and secondarily to provide adequate thrust to prevent loss of control in normal flying conditions. Hovering or near hovering was chosen as the primary goal, because it is the worst-case scenario for propeller efficiency as a result of the lack of air inflow. A method was developed to determine optimized airfoils for a range of angles of attack and at varying Reynolds numbers. Describing airfoil geometry during optimization can be a complicated task because of the high number of required points along the surface to show the changing curves. Varying methods exist to perform this task, such as a general coordinate system for each point, a Parsec method that uses different variables for curves and radii, or the class function / shape function transformation technique, CST, developed by Kulfan [16] that uses a number of variables while employing Bernstein polynomials. Each method has its advantages, but the CST method was used because of the geometry requirements of the program used to generate the lift and drag coefficients. The airfoil geometry was tested in Xfoil [17] to determine the best lift-to-drag ratios over the varying angles of attack. Xfoil is a program created by the Massachusetts Institute of Technology (MIT) to specifically analyze low Reynolds number airfoils. MATLAB was used to drive the main optimization of the airfoil, which was done by using a hybrid pattern and particle

swarm method to track and change the airfoil geometry and then test each shape in Xfoil to determine performance. The highest performing airfoil geometry was saved for future analysis. The optimization program runs at four different Reynolds numbers – 100,000, 200,000, 318,000, and 360,000 -- that were obtained by estimating the chord lengths and propeller blade lengths, and solves for airfoils at angles of attack ranging from zero to nine degrees. This program provides thirty-six different airfoils to be tested for propeller efficiencies. The lift and drag curves were generated for each airfoil and then run through a MATLAB propeller optimizer that determines the best propeller blade based on pitch, chord length, taper and length. The propeller analysis was conducted using a combination of blade element theory and moment theory, modified to work with aircraft in a hovering condition.

For the airfoil and propeller generation portion of the project, airfoils have been optimized to provide a lift-to-drag ratio of 90 or above depending on the Reynolds number and angle of attack. The propeller optimizer is able to work with the large range of airfoils by having the ability to change multiple propeller characteristics. The efficiency of the designed propellers, which is measured as a function of the coefficient of thrust versus the coefficient of power, is in the range of 60 to 83 percent. Two propellers were chosen from the higher performing designs to be modeled in Solidworks. These models were then imported into the Solidworks Flow Simulation software, which allows for a computational fluid dynamic (CFD) analysis to be conducted. This method of analysis provides a close approximation to how the propeller will work based on calculations of fluid cells around the geometric shape. The results from the CFD analysis were compared to the theoretical values provided from the MATLAB program to verify the efficiency accuracy of the designed propellers. The final step performed was a finite element analysis (FEA) of the

designs while rotating the propeller at the maximum RPM to determine if they would structurally fail under the loads.

## Background

The issue of small-scale, low-Reynolds-number propellers with low efficiencies has been known since near the beginning of large-scale airfoils for propeller testing [6, 8, 9, 18]. This issue was first discovered when large discrepancies were observed in the expected efficiency from theoretical models and large models to the smaller models. As airfoils were being tested in wind tunnels to determine the lift-to-drag ratios, smaller models were used at different airspeeds to compress the air to help overcome the scaling effect from the small models to the full-sized propellers. At the very small chord length and low forward air velocity, the Reynolds number would become low enough to cause the maximum lift-to-drag ratio to lower more than expected [6, 9, 13, 18]. This was caused by an increase in the drag due to the flow of air over the airfoil. To help overcome this issue, larger propellers were tested or the kinematic viscosity was changed to keep the Reynolds number at a higher level and thereby remove the error [6, 9, 18]. For MAVs, the limitations of increasing the propeller to a larger size prevent it from achieving the higher Reynolds numbers to lower drag.

Current research in the use of low-Reynolds-number airfoils and propellers has been kept to a mostly academic level at this time [11, 12, 19, 20, 21, 22, 23, 24, 25]. Most of the academic papers have focused on existing small-scale propellers to determine if the blade element momentum theory, BEM, theoretical values match the ones measured in wind tunnel tests. This has been mostly accurate when compared to the results and is important in proving that the equations used for large-scale propellers work for the small-

scale as well. However, these papers have had some common setbacks in gaining optimal results for comparison. For example, there have been issues concerning the testing methods, which have sometimes led to less accurate results. Some of these cases have involved vibrations in the test equipment, calibration issues in the sensors and other wind tunnel related issues. To overcome these setbacks, most of the test jigs now feature a test procedure to verify that the data match data results from a solved small-scale airfoil before proceeding with different propellers [11, 12, 23]. Another issue that has been pointed out in the research is the lack of airfoil data provided by the manufacturers. This situation has led to a couple of methods to try to determine the airfoil shape. The most promising method at this time is the use of photographs of the propeller in two different orientations, which are then employed to calculate the angles [26]. Software called PropellerScanner from Dr. Hepperle [25] can perform this action by analyzing scans of a propeller. This method combined with the BEM in one study [26] provided accuracy in the range of 10 to 20 percent, with respect to the physical testing, but because the BEM method has its own range of accuracy, it is difficult to determine how accurate the PropellerScanner is. There has not been any testing done solely to determine the accuracy of the software at this time.

Another branch of research has focused on modifying existing large-scale airfoils to help overcome the increased drag at the smaller scale. In most of these research papers, the propeller is solved only to the point of general efficiency comparisons of theoretical to experimental and for general applications. An example of this procedure is in a paper written by Deters, Ananda and Selig [26], in which they design and test a modified Clark-Y airfoil, named NR640. With testing, they were able to achieve about a 70% efficiency. A method tested by Parthapanayaka, Vinod and Krishnamurthy [21] involved combining two

known large-scale propellers, an Eppler-193 and a NACA 66-021, to gain desired flight characteristics while meeting the stresses added to the modified propeller. This allowed the propeller to achieve 76% efficiency for a cruise condition. The Parthapanayaka, Vinod and Krishnamuthry design was made specifically for a NAL MAV at a set operating condition, while the Deters, Anada and Selig design was tried at a couple of varying diameters, pitches and number of blades. With a few exceptions, most of the papers following this line of research are only based on a single desired design for a specific aircraft or on arbitrarily chosen design inputs to determine how well the design method works. This research is helpful in showing that higher efficiencies are possible despite the low Reynolds number operating condition. However, these projects are not set up in a manner that would assist a designer in making a new product that did not meet the same inputs and desired outputs.

A very small number of research papers have attempted to model their own propellers using existing airfoil data from the National Advisory Committee for Aeronautics (NACA), which was the precursor for NASA [27]. The NACA provided most of the airfoil data through testing of different shapes and is still used today for many airfoil designs. Based on papers from the NACA and NASA [7, 8, 18], low Reynolds numbers have been tested on the existing airfoils and they have a very low efficiency. Because the airfoil used in this testing had low efficiency, the propellers tested in these papers had an efficiency of 65 percent or lower.

If a method was devised that used a combination of modified airfoils specifically designed for low Reynolds number flight and propellers designed using these airfoils with the capability of changing application-specific inputs, a baseline could be provided to show

how to increase overall efficiency. This development would provide a starting point for designing further application-specific propellers, without randomly guessing about the performance of a propeller, which might only get a UAV close to desired flight characteristics.

Currently, two attempts have been made to design airfoils and propellers specifically for low-Reynolds-number applications. The first attempt was by Wall [24] and the second attempt was by Rutkay [19]. These papers used the BEM with vortex methods and Xfoil to solve for a range of values using optimization methods. The propellers studied were for fixed wing forward flight aircraft. The forward flight aircraft have the benefit of increasing efficiency with a higher forward velocity. The propellers were optimized to work in varying conditions, such as climbing and cruise. In both papers, the research work resulted in higher efficiency propellers than the off-the-shelf baseline ones tested.

## Basics of Airfoils

A propeller is basically a wing that has been twisted, and the cross-section of a wing is made up of an airfoil. An airfoil is a curved shape that produces a low-pressure zone on the upper surface and a high-pressure zone on the lower surface when a fluid is flowing around the shape from front to back. The difference in pressures creates a normal, $N$, and axial, $A$, force on the airfoil, which can be broken into lift, $L$, and drag, $D$, components. The lift component is in the direction of the low-pressure zone and is perpendicular to the freestream, $V_\infty$, flow of fluid. The drag component is parallel to the freestream flow of the fluid. The airfoil is placed at some angle to the freestream flow, which changes the amount of lift and drag produced by the airfoil. This angle is referred to as the angle of attack, AOA or $\alpha$. The chord, $c$, of the airfoil is a line drawn from the front

part of the airfoil to the back edge. The forces and components are shown in Figure 2.

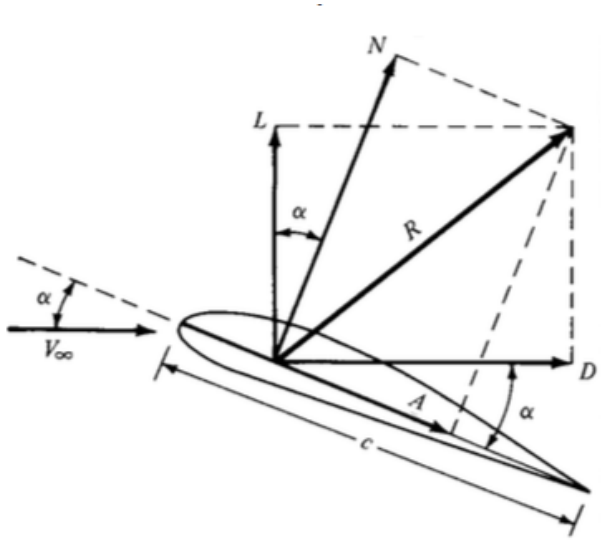


**Figure 2: Airfoil Force Components [13].**

The basic lift and drag values are obtained with Equations (5) and (6) , which show how the angle of attack and varying forces affect the values [13]:

$$L = N * \cos(\alpha) - A * \sin(\alpha), \quad (5)$$

$$D = N * \sin(\alpha) + A * \cos(\alpha). \quad (6)$$

To allow for easier comparison of airfoils, a dimensionless coefficient of lift and drag are normally used to describe the airfoil characteristics. These coefficients are denoted by $C_l$ for lift and $C_d$ for drag. All airfoils are described by a set of geometric features. The chord is the line drawn from the leading edge to the trailing edge of the airfoil. The leading edge is the front-most part of the airfoil, while the trailing edge is the most rearward point. The mean camber line splits the upper and lower surface of the airfoil into equal parts. The camber is the maximum distance between the mean camber line and the chord line. The upper and lower surfaces of an airfoil can be mirrored, making the airfoil symmetric or

featuring different shapes, depending on the desired lift and drag coefficients. A positive camber airfoil has the mean camber line above the chord line. Figure 3 shows the parts of an airfoil with a positive camber.

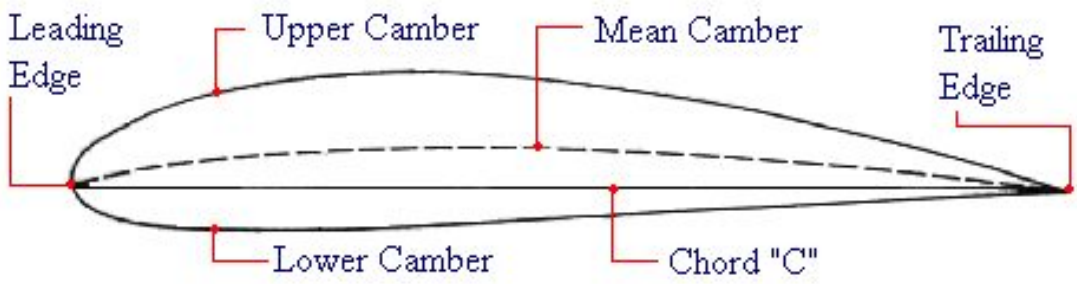


**Figure 3: Parts of an Airfoil [28].**

Airfoil shapes can be described in many ways, such as individual coordinate points along the curves, the Parsec method -- which assigns different variables to radii and curves -- or the CST method. The standard airfoil description for large-scale airfoils is the NACA standard. The airfoils can be described by a 1-, 4-, 5-, 6-, 7- or 8-series number, such as NACA 2421. For each series, the numbers and their locations in the airfoil description provide a different meaning for the geometry. Using the NACA 2421 as an example, the first digit is the maximum camber, the second digit is the location of the maximum camber along the chord from the leading edge, and the last two digits are the maximum thickness. In this example, the maximum camber is 2% of the chord, located at 40% of the chord length, with a maximum thickness of 21%. Equations (7), (8), (9), (10), (11), and (12) are used to obtain the upper and lower geometries from the NACA four digit series [29, 30]:

$$y(t) = \frac{t}{0.2}\left(0.2969\sqrt{\frac{x}{c}} - 0.1260\frac{x}{c} - 0.351\left(\frac{x}{c}\right)^2 + 0.2843\left(\frac{x}{c}\right)^3 - 0.1015\left(\frac{x}{c}\right)^4\right), \quad (7)$$

$$X_u = x - y_t sin\theta, \quad (8)$$

$$Y_u = y_c - y_t cos\theta, \quad (9)$$

$$X_l = x + y_t sin\theta, \quad (10)$$

$$Y_l = y_c + y_t cos\theta, \quad (11)$$

$$\theta = tan^{-1}(\frac{dy_c}{dx}). \quad (12)$$

These equations are very useful if the designer is choosing a known NACA airfoil to determine the coordinates of the geometry for modeling. Unfortunately, these equations do not work well for optimization methods because they do not allow for an easy change of geometry when testing many different airfoil shapes. After an airfoil optimization is complete, the geometry of the airfoil can be converted back to a NACA standard and then compared to existing airfoil data for verification of the shape.

To allow for an easier optimization of the airfoil, the CST method was used to generate the airfoil geometry. For input geometry, Xfoil needs very smooth curves to be able to efficiently solve for the coefficients of lift and drag. If less than optimal geometry is input into the program, it will provide a non-convergence error for the solution, unless a high number of iterations are used. A high number of iterations in Xfoil will greatly increase the solving time for each airfoil tested. The CST method was developed by Kulfan [16] to easily use Bernstein polynomials and Bezier curves to describe an airfoil with varying numbers of inputs. A Bezier curve uses Bernstein polynomials to determine the control points for the curves, and while ranging from 0 to 1. Equation (13) shows the Bezier curve equation and Equations (14) and (15) are for the Bernstein polynomial [31, 32]:

$$B(t) = (1-t)^3 B_0 + 3(1-t)^2 t B_1 + 3(1-t)t^2 B_2 + t^3 B_3, \quad (13)$$

$$B(t) = (\frac{n}{i})t^i(1-t)^{n-i}, \quad (14)$$

$$\left(\frac{n}{i}\right) = \frac{n!}{i!(n-i)!}. \quad (15)$$

The t value ranges from 0 to 1 and the B values are the control points for the coordinate locations. The upper section of the airfoil requires at least two Bezier curves to describe it as well as the lower section. The first point in the first Bezier curve is attached to the leading edge and the last point is set to the maximum camber. The first point in the second Bezier curve is set to the maximum camber and the last point is set to the trailing edge. The remaining four points are used to manipulate the curves to meet the desired geometry. This method allows for a simple method to determine airfoil geometry, but in its current form, it is hard to use for an optimizer.

As the CST method uses Bezier curves, the airfoil is solved in two parts, first for the upper and then the lower sections. The basic equation [16] for the CST is method is shown in Equation (16):

$$\xi(\psi) = \sqrt{\psi}(1-\psi)\sum_{i=0}^{N} A_i\psi^i + \psi\xi_t, \quad (16)$$

where $\Psi$=x/c, $\zeta$=z/c, and $\zeta t$=$\Delta\zeta$TE/c. Psi is the step location along the chord length, $x_i$ is the z location of the curve along the chord length, and the delta $x_i$ is the change in the trailing edge thickness over the chord length. The shape function is shown in Equation (17):

$$S(\psi) = \sum_{i=1}^{n} A_i S_i(\psi), \quad (17)$$

where $S_i$ is the shape function, $Ai$ is the unknown coefficient for the curve, and Psi is the step along the chord length. The shape function is determined using the Bernstein polynomial and is set to an order of 6. Equations (18) and (19) show the shape function equations:

$$S_{(r,n)}(x) = K_{r,n}x^r(1-x)^{n-r}, \tag{18}$$

$$K_{r,n} = \frac{n!}{r!(n-r)!}. \tag{19}$$

Increasing the order of the Bernstein polynomials will increase the control over the shape of the airfoil, because it uses more curves to describe the overall shape. The disadvantage to using a higher order is it will greatly increase the processing time for the optimizer because of the higher number input variables. Figure 4 shows the Bernstein polynomial curves at different orders.

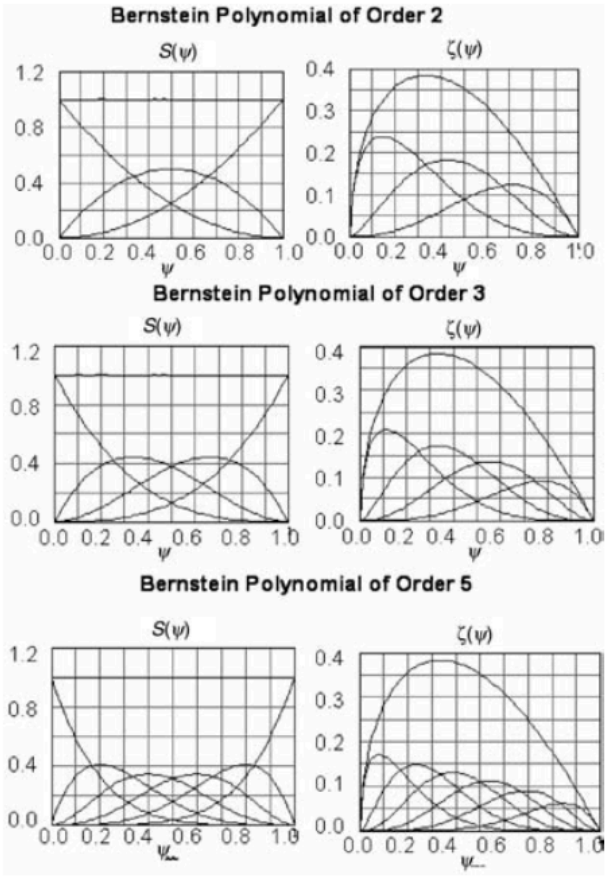


**Figure 4: Bernstein Polynomial Curves [16].**

A class function is used to allow user control over the general shape of the airfoil to set it to meet the required flight parameters. An example is getting a rounded nose and

sharp trailing edge airfoil for subsonic flight or a wedged-shape airfoil for supersonic flights. The class function equation is shown in Equation (20):

$$C_{N2}^{N1}(\psi) = \psi^{N1}(1-\psi)^{N2}. \quad (20)$$

Table 1 shows the possible inputs into the class-shape function and what type of airfoil output the function will provide.

**Table 1: Class Function Inputs.**

| N1 | N2 | Airfoil Description |
|---|---|---|
| 0.5 | 1.0 | Round nose and pointed aft end |
| 0.5 | 0.5 | Elliptic or and ellipsoid body of revolution |
| 1.0 | 1.0 | Biconvex or ogive body |
| 0.75 | 0.75 | Sears-Haack Body (minimum drag supersonic body) |
| 0.75 | 0.25 | Low-drag projectile |
| 1.0 | 0.001 | Cone or wedge |
| 0.001 | 0001 | Rectangle, circular duct, or a circular rod |

Replacing parts of the original Equation (16) with the shape function and the class function Equations (17) and (20) provides the final equation for the CST method. This is shown in Equation (21):

$$\xi = C_{N2}^{N1}(\psi)\sum_{i=1}^{n} A_i S_i(\psi) + \psi\Delta\xi_t. \quad (21)$$

For a 6th order Bernstein polynomial, a total of fourteen *A* value inputs will be needed to draw the airfoil shape, seven for the upper curve, and seven for the lower curve. An example of the method is shown Table 2, which has the input values, and Figure 5, which shows the airfoil.

**Table 2: CST Method Example Inputs.**

| i | 1 | 2 | 3 | 4 | 5 | 6 | 7 |
|---|---|---|---|---|---|---|---|
| A upper | 0.2284 | 0.600 | 0.2085 | 0.3668 | 0.4238 | 0.3732 | 0.4113 |
| A lower | -0.0038 | 0.1806 | -0.0129 | 0.1989 | 0.1978 | 0.1997 | 0.1999 |

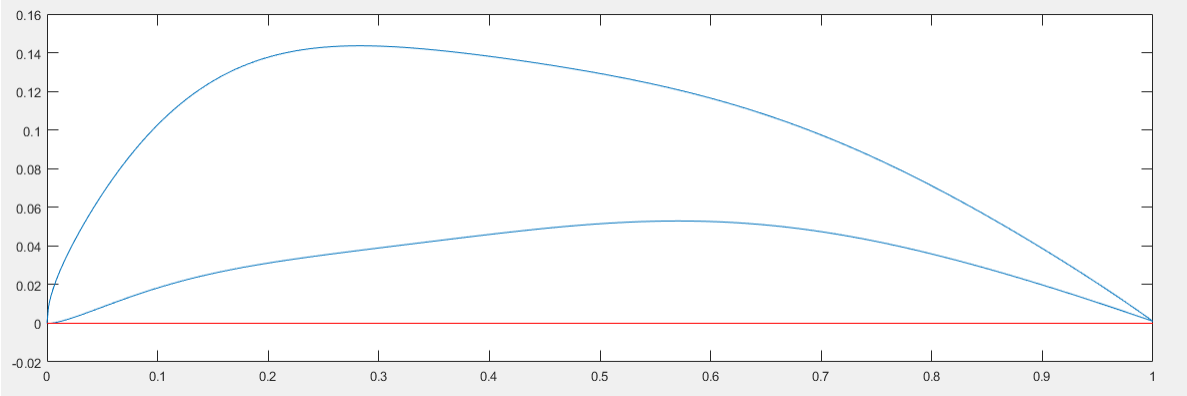


**Figure 5: CST Airfoil Example.**

## Basics of Propellers

A propeller, like a wing, creates lift as it moves through a fluid. The propeller blade generates lift as it rotates and it is called thrust. The cross-section of a propeller closely resembles the cross-section of the standard airfoil as it has a coefficient of lift and drag based on the angle of attack, freestream velocity and the resultant forces. However, as the blade is rotating at an angle and at a varying speed along the blade, other forces must be included. The rotational velocities affect the lift of the blade and the twist or pitch of the blade changes the effective angle of attack. Common propellers include two to four blades. Airfoil terms are the same for either a wing or a propeller, such as chord, angle of attack, mean camber line and others. The section that connects the propeller to the motor or transmission is called the hub. The root of the blade is where the blade is connected to the

hub and usually occupies the first 20% of the total blade radius. The tip of the blade is the end furthest away from the hub. Figure 6 shows the basic parts of a propeller.

Modern day propeller design is still based on classical theories of air momentum, blade shape, and advancement of the blade compared to the flow of air [10, 11, 12, 18, 19, 26]. These original theories were based on steady state airflow conditions to assist in the ease of deriving solutions that closely described the physical test results. As time progressed, new correction factors and modifications to the original theories provided more accurate results. The theories used in propeller design are the momentum theory, the blade element theory (BEM), and the vortex theory [9].

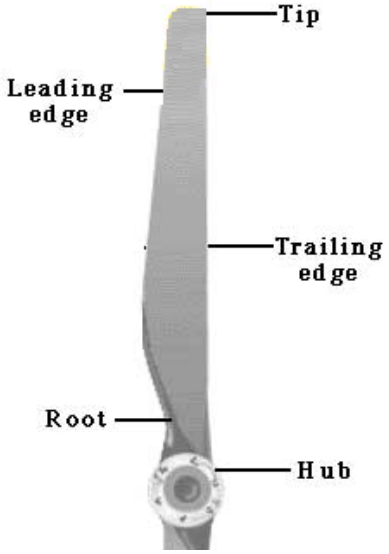


**Figure 6: Parts of a Propeller.**

Rankine and Froude developed the simple momentum theory and it is based on the kinetic energy and momentum imparted to the flow of air [9]. The propeller is assumed to be an advancing thin disc, an actuator disc, and it produces a uniform thrust, T, on a flow of air. The thrust causes the air pressure to be lower in front of the disc than behind the disc. This theory assumes that there is an infinite number of blades, the air is incompressible, the static pressure is equal upstream and downstream far from the influence of the actuator

disc, and there is no frictional or pressure drag from the blades [9]. Figure 7 shows a diagram of the momentum theory.

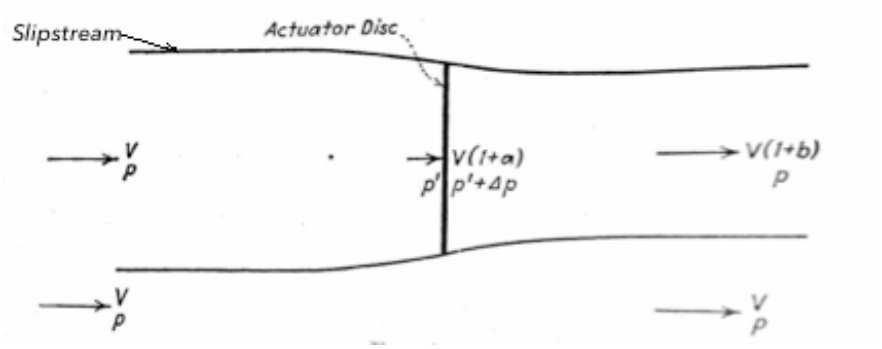


**Figure 7: Momentum Theory [9].**

The airstream, where not affected by the actuator disc, has the velocity, *V*, and the static pressure, *P*. The lowered pressure, *p'*, is in front of the disc and the higher pressure right after the disc is *p'*+ Δp. *V+Va* gives the velocity right after and through the disc and *V+Vb* gives the velocity after the pressure has reached equilibrium. The *V+Vb* is due to the increase of velocity caused by the slipstream as the pressure returns to the static pressure. The Bernoulli equation can be used to calculate the change in pressure, and is shown in Equations (22) and (23):

$$H = p + \frac{1}{2}\rho V^2 = p' + \frac{1}{2}\rho V^2(1+a)^2 \qquad (22)$$

and

$$H1 = p + \Delta p + \frac{1}{2}\rho V^2(1+a)^2 = p + \frac{1}{2}\rho V^2(1+b)^2\,. \qquad (23)$$

The head, *H*, for the front of the disc is given by Equation (22) and at the rear of the disc by Equation (23). The thrust is determined by the difference in pressure from the front of the

disc to the back [9]. Combining Equations (22) and (23) gives the change in pressure. The thrust is the total area of the disc multiplied by the change in pressure. Thus,

$$\Delta p = H1 - H = \rho V^2 b \left(1 + \frac{b}{2}\right) \tag{24}$$

and

$$T = A\rho V^2 b \left(1 + \frac{b}{2}\right). \tag{25}$$

As thrust is also equal to the change in axial momentum over time, it can also be described as mass per unit time times the velocity imparted [9]. Therefore,

$$T = AV(1 + a) * \rho bV = A\rho V^2 b(1 + a). \tag{26}$$

As both Equations (24) and (25) equal thrust, setting the equations to each other gives Equation (8) and the result in (27) and (28):

$$A\rho V^2 b \left(1 + \frac{b}{2}\right) = A\rho V^2 b(1 + a) \tag{27}$$

and

$$a = \frac{b}{2}\ . \tag{28}$$

According to the momentum theory, half of the velocity is added to the slipstream before the actuator disc and the other half after [9]. The ideal efficiency of a propeller can be calculated from the momentum theory; it is a function of the thrust and velocity compared to the kinetic energy increase in the fluid [9]. Thus,

$$Kinetic\ Energy = pAbV^3(1 + a)^2 \tag{29}$$

and

$$Efficiency = \eta = \frac{T*V}{pAbV^3(1+a)^2} = \frac{pAbV^3(1+a)}{pAbV^3(1+a)^2} = \frac{1}{1+a}\ . \tag{30}$$

The ideal efficiency is not an accurate representation of the actual efficiency, because of the assumptions associated with the theory, but it provides a benchmark that can be useful for attempting to get as close as possible.

The momentum theory provides another set of useful information for propeller design guidelines. If the efficiency, thrust coefficient, *Ct*, and difference in velocity -- Equation (28) -- are combined, the results include Equations (31), (32), (33), and (34):

$$T = \frac{2\rho A V^2(1-\eta)}{\eta^2}\,, \tag{31}$$

$$C_t = \frac{T}{qA}\,, \tag{32}$$

$$q = \frac{1}{2}\rho V^2\,, \tag{33}$$

and

$$\frac{\eta}{1-\eta} = \frac{4}{C_t}\,. \tag{34}$$

Equation (34) is used to determine the ideal efficiencies with a changing thrust coefficient. From this equation, the four basic design principles can be determined [9]. Ideal efficiency decreases with the increase of thrust. The ideal efficiency increases with an increase in forward velocity, with an increase in the density of air and with an increase in the propeller diameter.

As the momentum theory determines the thrust based on a generalized propeller disc, without taking into consideration the torque on the propeller or the thrust varying over the length of the blade, another method must be used that includes these and other factors. The blade element method cuts the blade of a propeller into small sections and each section is individually analyzed to determine its aerodynamic properties [9]. It is assumed for this method that the propeller is a twisted airfoil, and as such, each section is considered a two-

dimensional (2D) airfoil for the calculations [9]. These sections are then combined to determine an overall propeller performance. Figure 8 shows the front view of the propeller and how a section of the airfoil is sliced.

The initial blade element theory did not include the induced down flow, the interference between the propeller blades, and the tip loss [9]. The simple form of this method is good for overall estimations, but not very accurate, and is unsuitable for design.

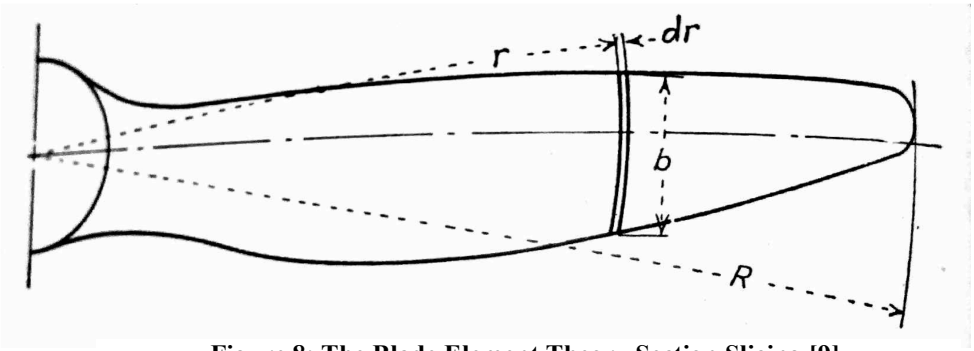


**Figure 8: The Blade Element Theory Section Slicing [9].**

The simple blade element theory was modified to include various correction factors and to include information from the momentum theory to be used in its current state. The modified method is the combined momentum and blade element theory (BEM) [9]. Figure 9 shows the position of a section of airfoil with the corresponding forces and relative angles required to use the BEM.

The first step in this method is to determine the solidity factor, *S*, as it applies to charts determined from wind tunnel testing to apply correction factors:

$$S = \frac{2\pi r}{Bb} \quad . \tag{35}$$

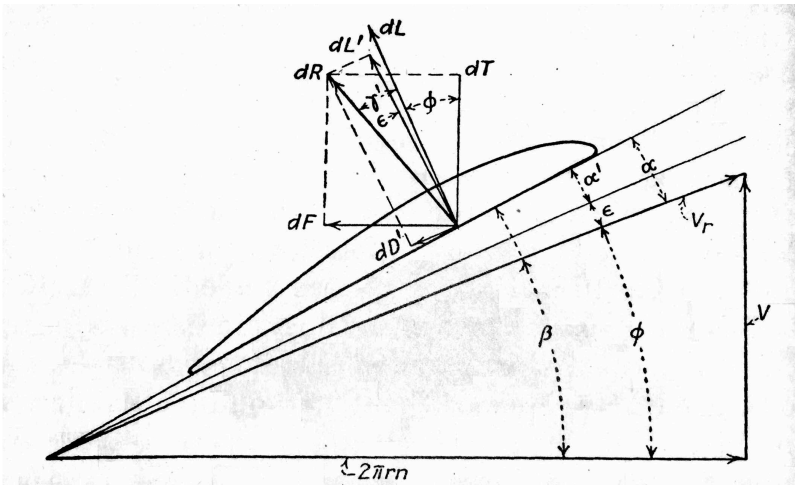


**Figure 9: The BEM Airfoil Section [9].**

The *r* is the radius at that section of study, *B* is the number of blades, and *b* is the blade width. The thrust is calculated [9] by Equations (36), (37), (38), (39), and (40):

$$T = \frac{1}{2}\rho V^2 B \int_0^R T_c dr \ , \tag{36}$$

$$T_c = K * \cos(\phi + \gamma') \, , \tag{37}$$

$$K = \frac{C_{l'} b}{sin^2\phi * \cos\,(\gamma' - \epsilon)} \ , \tag{38}$$

$$y' = \arctan\,((\frac{D}{L})_{\alpha'} + \tan\,(\epsilon)) \tag{39}$$

and

$$\alpha' = \alpha - \epsilon \, . \tag{40}$$

The correction factor, $\epsilon$, is found from the tables based on the *S* and angle, $\phi$, in between each blade step. The torque on the propeller is calculated [9] with Equations (41) and (42):

$$Q = \frac{1}{2}\rho V^2 B \int_0^R Q_c dr \tag{41}$$

and

$$Q_c = Kr * \sin(\phi + \gamma') \ . \tag{42}$$

The efficiency of the element [9] is shown in Equation (43):

$$\eta = \frac{tan\phi}{\tan(\phi+\gamma')} \quad . \tag{43}$$

The correction factor tables are shown in Figures 10 and 11.

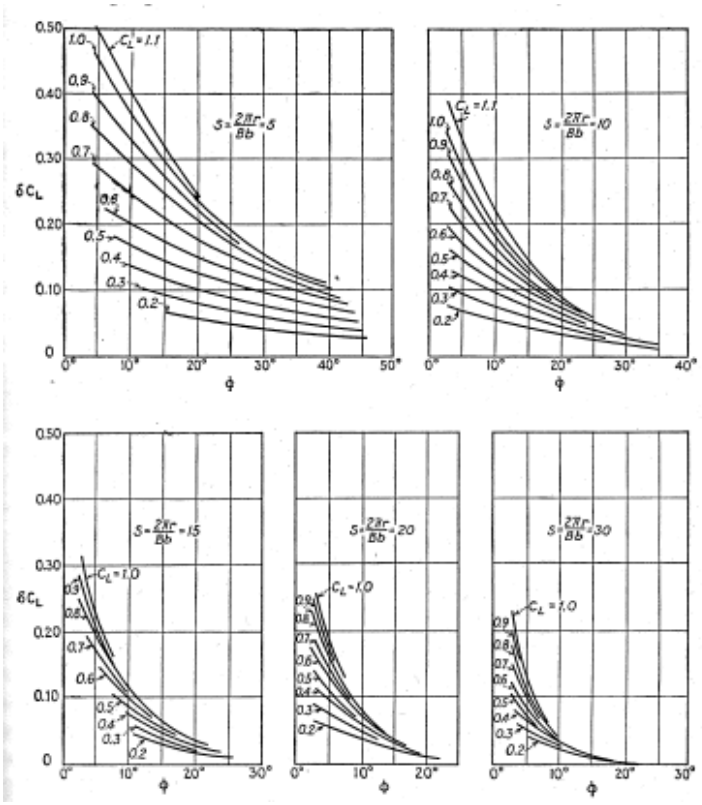


**Figure 10: Coefficient of Lift Correction Factor [9].**

This method as it is currently presented still assumes incompressible flows and steady state uniform air conditions. It does not include the tip correction or mach number correction factors [9]. These correction factors are multiplied by the results from the BEM to acquire a more accurate value of thrust, torque and efficiency by accounting for losses from the corresponding aerodynamic effects. The tip correction factor is given by Equation (44):

$$F = \frac{2}{\pi} cos^{-1}\left(e^{-\left(\frac{\frac{B}{2}*\left(1-\frac{r}{R}\right)}{\left(\frac{r}{R}\right)*sin\phi}\right)}\right) \quad . \tag{44}$$

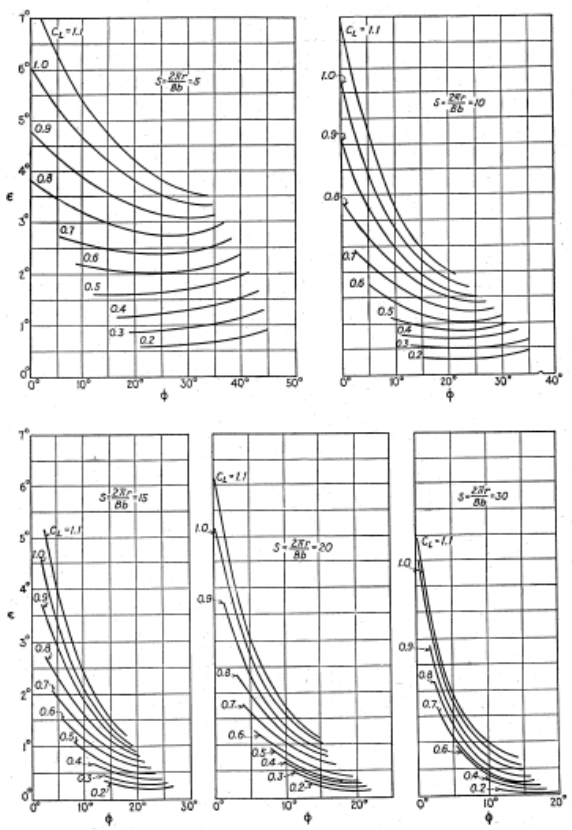

**Figure 11: Coefficient of Downwash Correction Factor [9].**

This is multiplied by Equation (36) to adjust the thrust provided from the propeller. This effect is caused by the loss of thrust near the tip because of pressure equalization. The mach number correction factor, provided by Glauert, is due to the increase of lift on low pitch propellers at a mach number below 0.6 [11]. Note that this method assumes the wing to be of an infinite length when solving for the airfoil section [9]. Thus,

$$C_L = \frac{C_{L,M=0}}{\sqrt{1-M^2}}\,. \tag{45}$$

The last method associated with propeller design entails adding the vortex theory to the BEM. This method is a combination of the vortex theory, which is used for calculating lift on an airfoil as a wing, with the previously described BEM [9]. This method calculates the lift based on the airfoil being a finite length and includes the interference caused by the

other blades. Figure 12 shows the position of a section of airfoil with the corresponding forces and relative angles required to use the BEM with vortex method.

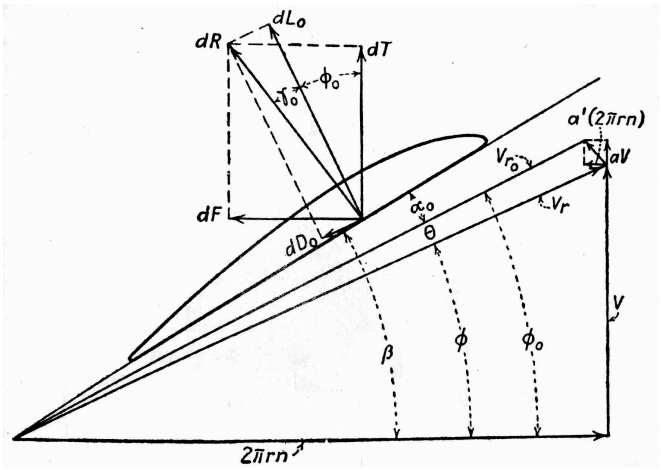


**Figure 12: The BEM Vortex Airfoil Section [10].**

The thrust and torque values are calculated from Equations (46) and (47) for each element from the vortex theory [9]. Thus,

$$dT = 4\pi\rho V^2(1+a)ardr \tag{46}$$

and

$$dQ = 4\pi\rho V(1+a)(2\pi rn)a'^{r^2}dr. \tag{47}$$

Adding the angles of the blade and angles of attack, the following coefficients of thrust, torque, and efficiency can be determined [9]. Therefore,

$$T = \frac{1}{2}\rho V^2 B \int_0^R T_c dr, \tag{48}$$

$$T_c = K * \cos(\phi_0 + \gamma_0), \tag{49}$$

$$K = \frac{C_l(1+a)^2}{sin^2\phi_0 * \cos\ \gamma_0}, \tag{50}$$

$$Q = \frac{1}{2}\rho V^2 B \int_0^R Q_c dr, \tag{51}$$

$$Q_c = Kr * \sin\ (\phi_0 + \gamma_0), \tag{52}$$

and

$$\eta = \frac{(1-a)'tan\phi_0}{(1+a)\tan(\phi_0+\gamma_0)}. \quad (53)$$

This method is an iterative process and has two methods of solving. The first method involves choosing multiple angles of attack, solving for the *a* and the *a'*, then the thrust and torque [9]. These values are then plotted, which allows the designer to choose the best values based on each angle of attack. The second method is to choose a reasonable angle for the interference, $\theta$, and then solve through an iterative process until the desired result is determined [9]. The second method is recommended for the accuracy of its results compared to experimental data [9]. The solidity factor, *S*, must be calculated to use on the provided figures from Equation (17). Three other factors need to be calculated for the iterations [9] as shown in Equations (54), (55) and (56):

$$\frac{S}{C_L} = \frac{1-tan\gamma_0\tan\theta}{4\sin(\phi+\theta)tan\theta}, \quad (54)$$

$$\frac{a}{1+a} = \frac{cot\phi_0(tan\phi_0-tan\phi)}{1+tan\phi\tan(\phi_0+\gamma_0)}, \quad (55)$$

and

$$1 + a = \frac{tan\phi_0[1+tan\phi\tan(\phi_0+\gamma_0)]}{tan\phi[1+tan\phi_0\tan(\phi_0+\gamma_0)]}. \quad (56)$$

Using these values in Figures 13 and 14 provides the modification numbers for the angle of attack for the iterative process.

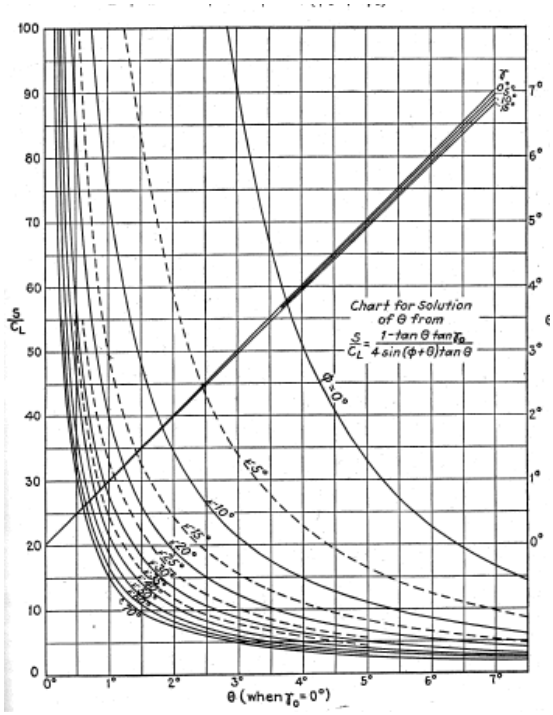


**Figure 13: Interference Angle with Solidity and Lift Ratio [9].**

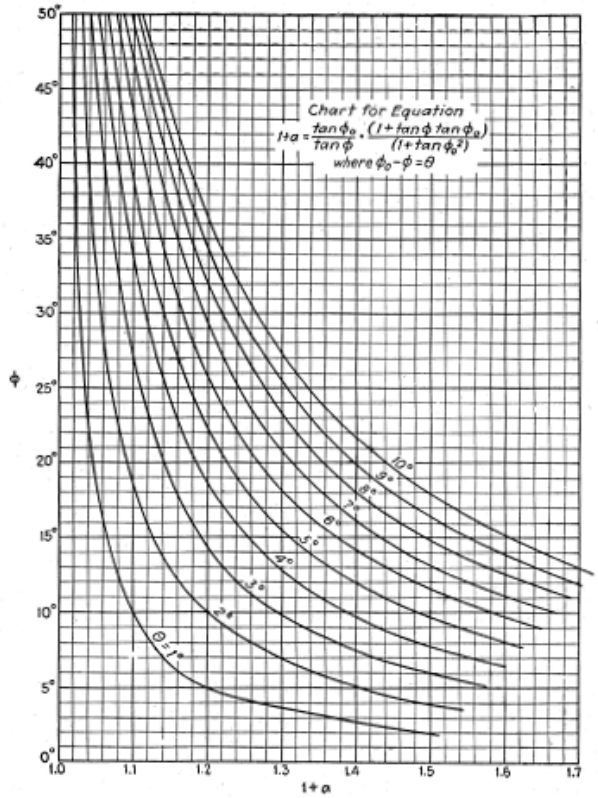


**Figure 14: Interference Angle and Angle of Attack Modifier [9].**

The tip and Mach number corrections can be applied to this method as well in the same manner as in the BEM. For the BEM and the vortex with blade element method, the airfoil coefficients of lift and drag are required. These values are determined based on the geometry of the airfoil, the angle of attack, the Reynolds number along the chord of the airfoil and the forward velocity [9].

For a multirotor to fly in a hovering or near-hovering state, the momentum theory and BEM have to be modified further, to be able to work with a near zero forward velocity. The BEM method for hovering conditions has a closed-form solution and an open-form solution depending on the design of the rotor blade and what assumptions are used. This method takes into consideration the slice of the blade being studied as well as the location of the blade in its circular path. Figures 15 and 16 show the blade section with the cross-sectional slice of the blade and the location on the path.

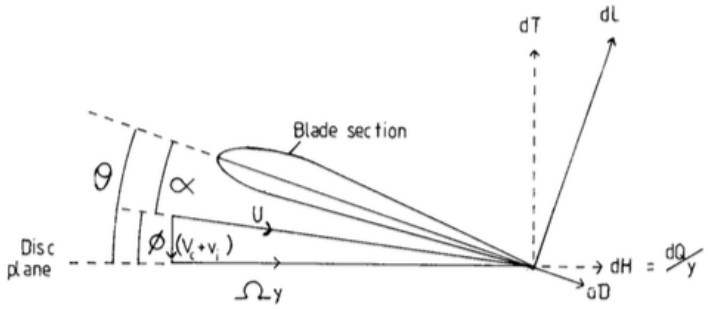


**Figure 15: Hover BEM Theory Cross-Section [33].**

The pitch of the rotor blade is denoted by $\theta$, the angle of incidence of the blade section is $\alpha$, the inflow angle is $\Phi$, and $U$ is the component velocity. Equations (57) and (58) are used to calculate lift and drag from the airfoil lift and drag coefficients. Component velocity is calculated from Equations (59), (60), and (61). All of the following equations were obtained and checked from three different resources to ensure accuracy [33, 34, 35]. Thus,

$$L = \frac{1}{2}\rho U^2 c C_l dr, \tag{57}$$

$$D = \frac{1}{2}\rho U^2 c C_d dr, \tag{58}$$

$$U = U_t + U_p, \tag{59}$$

$$U_t = \Omega * r, \tag{60}$$

and

$$U_p = V * \nu. \tag{61}$$

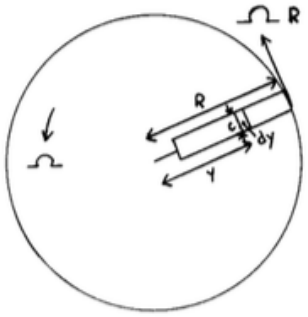


**Figure 16: Hover BEM Theory Rotor View [33].**

The angular velocity, $\Omega$, is in radians per second, $r$ is the sectional radius from the hub of the propeller, $V$ is the forward or upward velocity, and υ is the inflow velocity from the momentum equation. The angle of incidence or effective angle of attack is determined with Equation (62) and Equation (63):

$$\alpha = \theta - \phi, \tag{62}$$

$$\phi = U_p. \tag{63}$$

The overall thrust, $T$, for the propeller is calculated by determining the lift for each section along the length of the blade and then multiplying it by the number of blades. Equation (64) shows the thrust equation and Equation (65) shows the equation for torque:

$$T = N \int_0^R L dr, \tag{64}$$

$$Q = N \int_0^R (\phi L + D)\, r dr. \tag{65}$$

The thrust and torque are then converted to non-dimensional coefficients. This is shown in Equations (66) and (67). To simplify the equations, the coefficient of lift, $C_l$, is changed to the coefficient of lift at the angle of incidence, $C_{la}$, as shown in Equation (68). Thus,

$$C_t = \frac{T}{\rho * \pi * (\Omega R)^2}, \tag{66}$$

$$C_q = \frac{Q}{\rho * \pi * R (\Omega R)^2}, \tag{67}$$

and

$$C_{l\alpha} = C_l(\theta - \phi). \tag{68}$$

Simplifying Equations (66) and (67) gives the final open-form solution for coefficient of thrust and torque as shown in Equations (69), (70), and (71). For a hover situation, the coefficient of torque is the same as the coefficient for power. Thus,

$$\Delta C_t = \frac{N}{2 * \pi * R} \int_0^1 c * C_{l\alpha} \left[ \left( \frac{r}{R} \right)^2 \theta_r - \lambda_r \left( \frac{r}{R} \right) \right] dr, \tag{69}$$

$$C_t = \sum_{n=1}^{N} \Delta C_t, \tag{70}$$

and

$$C_p = C_q = \sum_{n=1}^{N} \lambda_n \Delta C_t. \tag{71}$$

In Equations (70) and (71), $N$, is the number of points being studied along the propeller blade. In Equation (69), $N$, is the number of blades on the propeller. The unknowns for these equations include the coefficient of thrust, $Ct$, the inflow factor, $\lambda$, and the blade pitch, $\theta$. The inflow factor must be estimated from the momentum theory by guessing an initial blade pitch and then iteratively solved with the BEM to determine the correct blade

pitch and inflow factor for a required coefficient of thrust. For a hover condition, the required coefficient of thrust can be calculated from Equation (66), as the thrust must equal the weight of the aircraft.

The momentum theory is modified because of the difference in inflow along the blade of the propeller and the location of the blade in the circular path, as shown in Figure 16. The thrust from the modified momentum theory is shown in Equation (72), and (73) shows the coefficient of thrust:

$$T = 2 * \rho * A * (V + v) * v, \tag{72}$$

$$dC_t = 4 * \lambda * \lambda_i * r * dr. \tag{73}$$

The coefficient of thrust for the momentum theory must match the coefficient of thrust from the BEM theory. Setting Equations (69) and (73) equal to each other, and solving for the inflow factor, provides Equation (74). Equation (75) is for the hovering condition. Therefore,

$$\lambda = -\left(\frac{\lambda_c}{2} + \frac{\sigma * C_{l\alpha}}{16}\right) * \sqrt{\left(\frac{\lambda_c}{2} + \frac{\sigma * C_{l\alpha}}{2}\right)^2 + \frac{\sigma * C_{l\alpha}}{8}\left(\theta\left(\frac{r}{R}\right) - \lambda_c\right)}, \tag{74}$$

$$\lambda_r = \frac{\sigma * C_{l\alpha}}{16} * \left(\sqrt{1 + \frac{32}{\sigma * C_{l\alpha}}\theta_r * r} - 1\right), \tag{75}$$

$$\lambda_c = \frac{V}{\Omega * R}, \tag{76}$$

and

$$\sigma = \frac{N * c}{\mathrm{R} * \pi}. \tag{77}$$

The efficiency of the propeller blade for hover is measured by the coefficient of thrust compared to the coefficient of power. The measurement of efficiency for the propeller is called figure of merit, FOM, and can only be used to compare propellers with blade loading values near each other. This means that a propeller from a larger aircraft with a bigger

motor cannot be compared to a much smaller aircraft motor, as the efficiencies would not correspond. The FOM equation is provided in Equation (78),

$$FOM = \frac{\frac{C_t^{\frac{3}{2}}}{\sqrt{2}}}{k*\frac{C_t^{\frac{3}{2}}}{\sqrt{2}}+\frac{\sigma*C_d}{8}}. \quad (78)$$

The profile power factor, *k,* is a factor added to account for losses in the motor to blade and for interference. The profile power factor is set to 1.15 based on experimental testing [33, 34, 35]. To account for root and tip losses, the coefficient of lift is only generated from about 20 percent of the radius to 97 percent of the radius, but the coefficient of drag is calculated along the entire length [34, 35].

## Methods

The optimization of the propeller has two main parts. First, multiple airfoils must be optimized at varying angles of attack and Reynolds numbers based on the maximum lift-to-drag ratio. Second, these airfoils must then be used to optimize a propeller based on varying diameters, chord lengths and motor speeds.

Before running an airfoil optimization program, some basic data needed to be obtained about the Iris+ Quadcopter, as shown in Figure 17, such as the weight, the existing motor data and the existing propeller measurement.

**Figure 17: Iris+ Quadcopter [36].**

These data are used throughout the optimization process as a starting point or goal for the optimizers. The weight of the aircraft is about 1650 grams and is about 1840 grams with a GoPro camera, transmitter, and battery. The clearance for the propeller from the motor to the body of the aircraft is 7 inches. The information on the motor is not available from the manufacturer's website, so to determine the motor RPM at a hovering state, a thrust test stand was used with a tachometer, as shown in Figure 18. This provided a value of 4750 RPM to meet the required thrust, 1840 grams divided by four, to keep the Iris+ at a hovering state. The motor is rated at 950kv, which means that at 11.1 volts, the Iris+ battery voltage level, the maximum unloaded RPM is about 10,450 RPM. Measuring the existing propeller at three points along the blade gave the chord length values of 12.5, 17, and 21mm. These were used to estimate the Reynolds numbers of 200k, 318k and 360k. The final Reynolds number of 100k was chosen to provide a low value for propeller optimization.

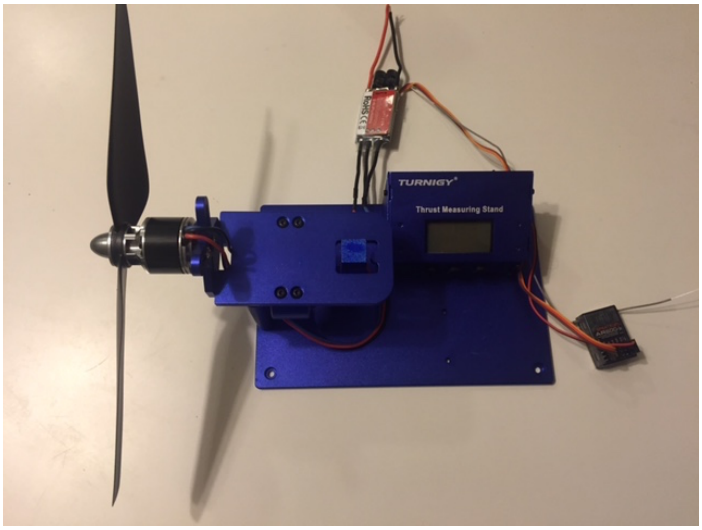


**Figure 18: Thrust Test Stand.**

The MATLAB program, which runs the various optimization programs, was separated into three parts. The first part optimizes the airfoils and then outputs a text file with the airfoil geometry and Reynolds number it was calculated at. The second part reads in the airfoil geometry text file and generates the coefficient of lift and drag curves for the airfoil over an angle of attack range of 0 to 15 degrees and then outputs another text file with this information. The last part of the program reads in the text file from the second program and optimizes the propeller based on the coefficients of lift and drag.

The first program uses a hybrid pattern search and particle swarm solver to modify the fourteen *A* variables used in the Kulfan CST method, within a range set by the user. The range for the variables at the most can be 0 to 1 or 0 to -1 based on the Bernstein polynomial, but setting the range to a closer desired value lowers the solving time for the optimizer. The objective function of the optimizer is set to find the maximum lift over drag value for the airfoil at the input angle of attack and Reynolds number. The main program runs angles of attack from 0 to 9 degrees at each of the four estimated Reynolds numbers. Initially, a particle swarm method was chosen to run the airfoil optimization portion of the program because of its ability to easily handle multiple variables and to not be susceptible to local minimum solutions. However, running the particle swarm method was very time and processor consuming. To lower the processing time to find a solution, a hybrid pattern search and particle swarm optimizer were used. The pattern search is a much quicker optimization method, but it can get stuck on a local minimum value [37]. The flow chart for the first program is shown in Figure 19.

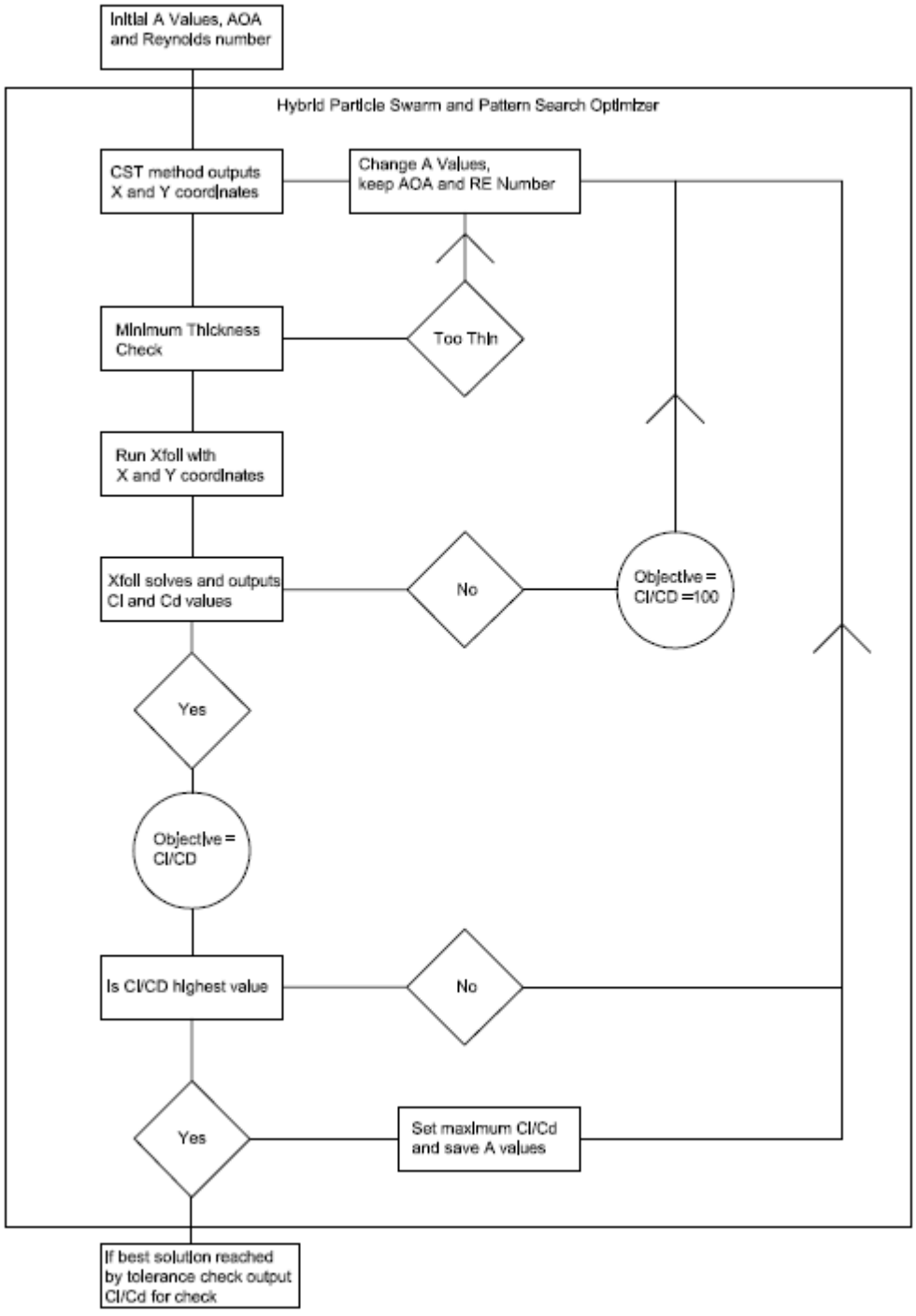


**Figure 19: Airfoil Optimization Flow Chart.**

After the program determined each optimized airfoil, it was output to a text file. This was done for three reasons. First, as a single airfoil could take over one hundred iterations to solve, which would take about 12 hours, the airfoils could be solved in chunks instead of one long run. Second, if the computer had an error, shut down, or if any other issue stopped the program, the data would not be lost nor would the program have to start from the beginning. Lastly, the next parts of the program could be solved at a later time without a delay.

The second part of the program read the text files from the first part of the program and then generated the full coefficient of lift and drag curves for angles of attack from 0 to 15 degrees with a step size of 0.2 degrees. This needed to be completed because the propeller optimization BEM theory method uses these coefficients, which change with the pitch of the blade. At times, Xfoil will be unable to determine a solution for an angle of attack because of limitations within the code. One possible solution in these cases is to increase the maximum number of iterations that Xfoil can use, but it can be very time consuming and may not provide a solution. Xfoil will also crash on some airfoil shapes at certain angles of attack. These issues will cause the coefficients of lift and drag to be missing some values as the program solves over the range of angles of attack. To account for this, the coefficient of lift slope is determined from the solved data points instead of individual values for the propeller optimizer. This method is normally used as the blade pitch does not typically have even angles of attack, depending on the number of points used along the blade. This method cannot be used with the coefficient of drag, because it does not follow a linear-sloped line. To determine the coefficient of drag, a Lagrange polynomial was used with the solved data points. This technique provided a reasonable

number for the coefficient of drag at different angles of attack. As with the first part of the program, the data were saved to a text file for each airfoil and Reynolds number.

The third part of the program runs an fminsearch optimizer using the airfoil data from the second part of the program at four different propeller diameters: 9, 10, 11, and 12 inches. The optimizer is set to determine the chord length, the chord taper along the blade, the motor RPM to run the propeller at the required hover thrust and the blade pitch. An fminsearch optimizer is used for this step because the range of possible solutions is very small and a local minimum will still meet the desired output. The objective for this optimizer is to determine the maximum FOM value. However, as the FOM can theoretically go to above 100 percent efficiency, the blade twist at the end of the blade is limited to 6 degrees. As the blade twist increases, the efficiency will continue to increase to an unrealistic number, because the theory does not account for blade stall. By limiting the twist at the end of the blade, it cannot reach the blade stall threshold. The propeller optimization flow chart is shown in Figure 20.

After obtaining the optimized propeller designs from the MATLAB code, two designs were chosen to model in Solidworks. These models were then imported into a CFD program to determine the thrust and torque at the specified RPM. This information was used to determine the propeller efficiency and to verify that the fluid flows were reacting to the propeller in an expected manner. The pressure results were then transferred to an FEA program to study the stresses on the propeller at the maximum motor RPM. This was used to determine if the design would fail under normal operating conditions and if anything needed to be modified in the design to correct for the problem.

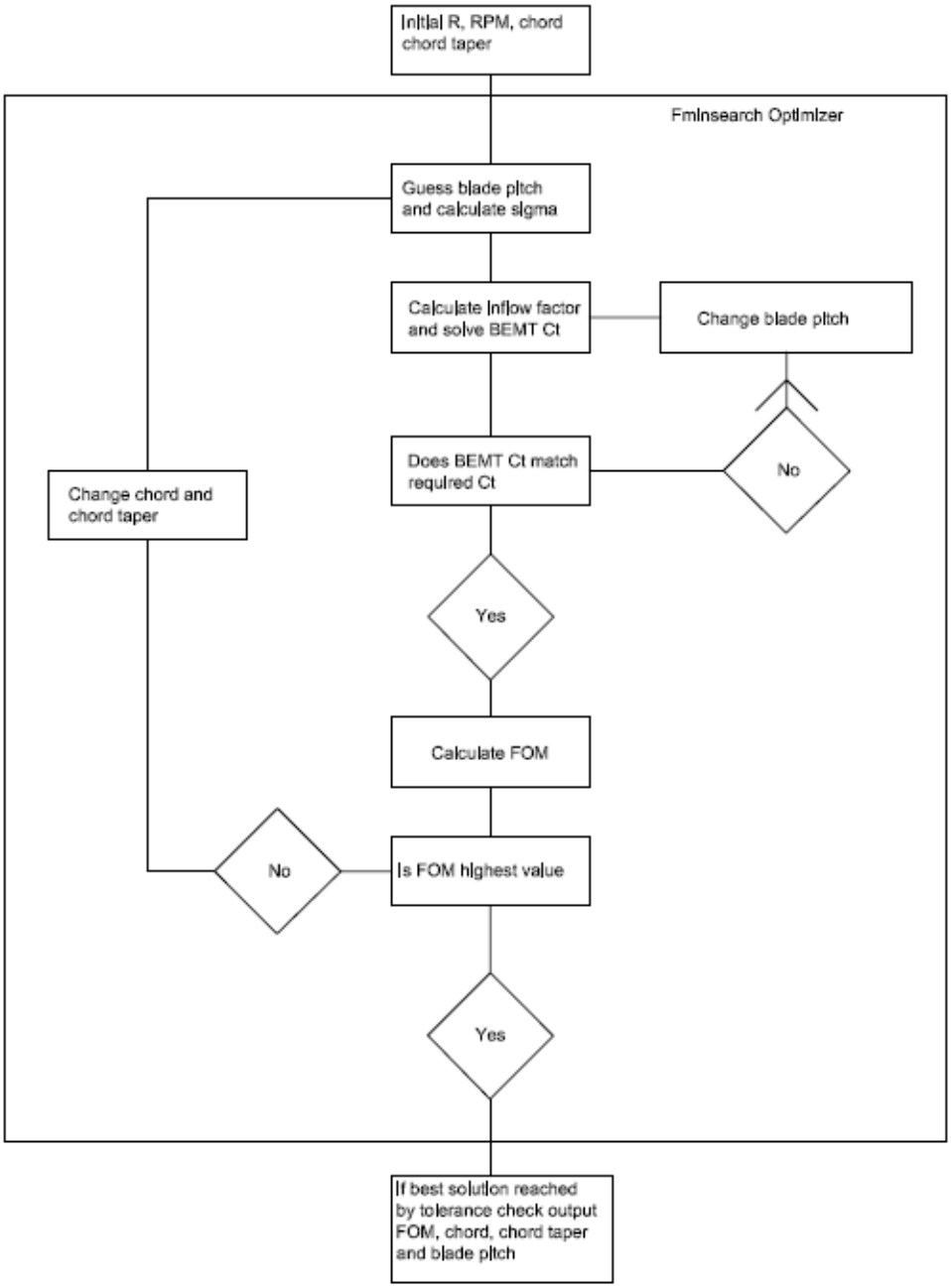


**Figure 20: Propeller Optimization Flow Chart.**

## Results

The propeller optimization code solved thirty-six airfoils over varying input parameters. The input parameters consisted of four different Reynolds numbers – 100,000, 200,000, 318,000, and 360,000 -- and nine different angles of attack from 0 to 8 degrees. Figure 21 shows an example of the text file outputs from the solver.

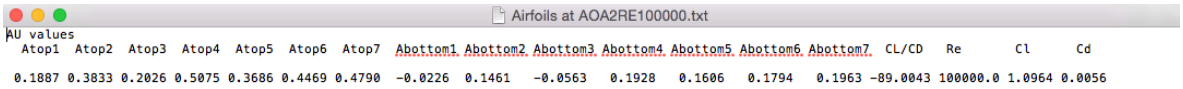


**Figure 21: Airfoil Optimizer Output File.**

Table 3 shows the A coefficients for airfoils at angles of attack 0 and 1, solving at each Reynolds number. An example only of the airfoil solutions was shown because the large size of the full output files.

**Table 3: Example of *A* Coefficients.**

| Angle of Attack | 0 | 0 | 0 | 0 | 1 | 1 | 1 | 1 |
|---|---|---|---|---|---|---|---|---|
| Reynolds Number | 100000 | 200000 | 318000 | 360000 | 100000 | 200000 | 316000 | 360000 |
| Au1 | 0.2659 | 0.5988 | 0.4423 | 0.2054 | 0.1979 | 0.2014 | 0.3713 | 0.1887 |
| Au2 | 0.3142 | 0.2297 | 0.3954 | 0.3972 | 0.5115 | 0.314 | 0.4799 | 0.3833 |
| Au3 | 0.4266 | 0.5597 | 0.2614 | 0.2943 | 0.3024 | 0.4476 | 0.2306 | 0.2026 |
| Au4 | 0.3256 | 0.2857 | 0.4779 | 0.2274 | 0.357 | 0.2448 | 0.3953 | 0.5075 |
| Au5 | 0.2868 | 0.4552 | 0.4529 | 0.4584 | 0.2897 | 0.5168 | 0.37 | 0.3686 |
| Au6 | 0.4405 | 0.479 | 0.3754 | 0.3427 | 0.4055 | 0.3255 | 0.3578 | 0.4469 |
| Au7 | 0.4966 | 0.4221 | 0.4049 | 0.3998 | 0.4648 | 0.4082 | 0.4058 | 0.479 |
| Al1 | -0.0318 | -0.0487 | -0.0302 | 0 | -0.0042 | -0.0308 | -0.0164 | -0.0226 |
| Al2 | -0.0122 | 0.0148 | 0.0459 | -0.0832 | 0.0433 | 0.0638 | 0.12 | 0.1461 |
| Al3 | 0.1275 | 0.0336 | 0.0517 | 0.125 | 0.0355 | 0.1987 | -0.1177 | -0.0563 |
| Al4 | 0.0358 | 0.0925 | -0.0312 | -0.1277 | 0.158 | -0.0084 | 0.1996 | 0.1928 |
| Al5 | -0.1012 | 0.0332 | 0.1977 | 0.1987 | 0.1093 | 0.1658 | -0.0476 | 0.1606 |
| Al6 | -0.0511 | 0.1971 | -0.282 | 0.1919 | -0.3148 | 0.1688 | 0.1821 | 0.1794 |
| Al7 | -0.1972 | 0.1994 | -0.3106 | 0.1999 | 0.1364 | 0.2 | 0.1982 | 0.1963 |

These *A* coefficients allow the airfoil geometry to be rebuilt into the x and y coordinate system, which was helpful for generating the coefficient of lift and drag curves. This method of storing the geometry also assists in the Solidworks modeling and analysis portion. The *Au* values represent the coefficients for the upper curve of the airfoil and the *Al* values are for the lower curve. A positive value means the curve is above the chord line and a negative value is below the chord line. Generation of the coefficients of lift and drag were from 0 to 15 with a step size of 0.2 for each airfoil. Table 4 shows a typical output file from this part of the program.

**Table 4: Example of $C_l$ and $C_d$ Output file.**

| Angle | $C_L$ | $C_D$ |
|---|---|---|
| 1 | 0.8646 | 0.0213 |
| 1.2 | 0.8895 | 0.0211 |
| 1.4 | 0.92 | 0.0207 |
| 1.6 | 0.9652 | 0.02 |
| 1.8 | 0.9932 | 0.0197 |
| 2 | 1.0222 | 0.0194 |
| 2.2 | 1.0513 | 0.0192 |
| 2.6 | 1.1079 | 0.0188 |
| 2.8 | 1.1357 | 0.0187 |
| 3 | 1.1547 | 0.0188 |
| 3.2 | 1.1766 | 0.0189 |
| 3.4 | 1.2011 | 0.0189 |
| 3.6 | 1.218 | 0.0191 |
| 3.8 | 1.24 | 0.0192 |
| 4 | 1.2561 | 0.0195 |
| 4.4 | 1.2916 | 0.0199 |
| 4.6 | 1.3109 | 0.0202 |
| 5 | 1.3435 | 0.0208 |
| 5.2 | 1.36 | 0.0212 |
| 5.4 | 1.3758 | 0.0216 |
| 5.6 | 1.3933 | 0.022 |
| 5.8 | 1.4116 | 0.0225 |

**Table 4: Example of $C_l$ and $C_d$ Output file (continued).**

| Angle | $C_L$ | $C_D$ |
|---|---|---|
| 6 | 1.4288 | 0.0229 |
| 6.2 | 1.4454 | 0.0234 |
| 6.8 | 1.4995 | 0.025 |
| 8.2 | 1.6172 | 0.0292 |
| 10 | 1.8536 | 0.04 |
| 12.8 | 1.497 | 0.065 |
| 13 | 1.485 | 0.0692 |
| 14.2 | 1.3298 | 0.1135 |
| 14.6 | 1.2911 | 0.1269 |
| 15 | 1.2503 | 0.1396 |

A review of Table 3 shows that angle of attack steps are missing from the 0 to 15 range. This will be discussed in the Xfoil issues section of the results. A typical airfoil coefficient of lift curve will rise from an angle of attack of 0, or less depending on the design, at a fairly linear rate until a certain angle of attack, and then progressively move downwards. The angle of attack for the peak coefficient of lift is dependent on the geometry of the airfoil. The typical airfoil coefficient of drag will start at a high point, small compared to the final drag, curve towards 0, and then increase slowly at first, and then rapidly at higher angles of attack. Figure 22 shows the coefficients of lift and drag for the airfoil optimized for a 5-degree angle of attack at a Reynolds number of 100,000. Figure 23 shows an example coefficient of lift and drag curve plot.

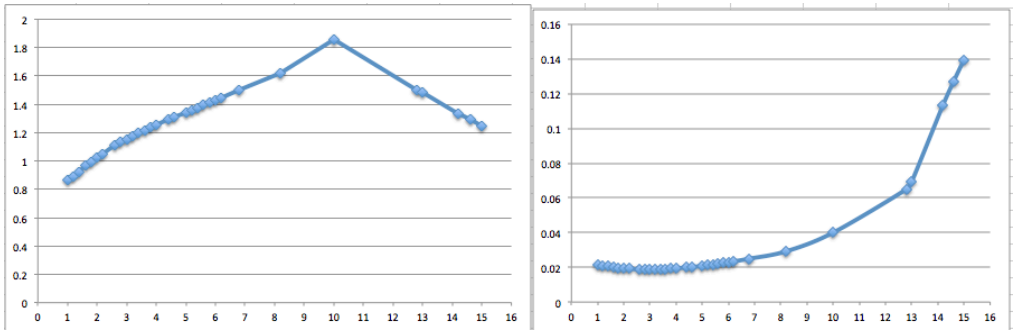


**Figure 22: Coefficient of Lift and Drag Curves for an Optimized Airfoil.**

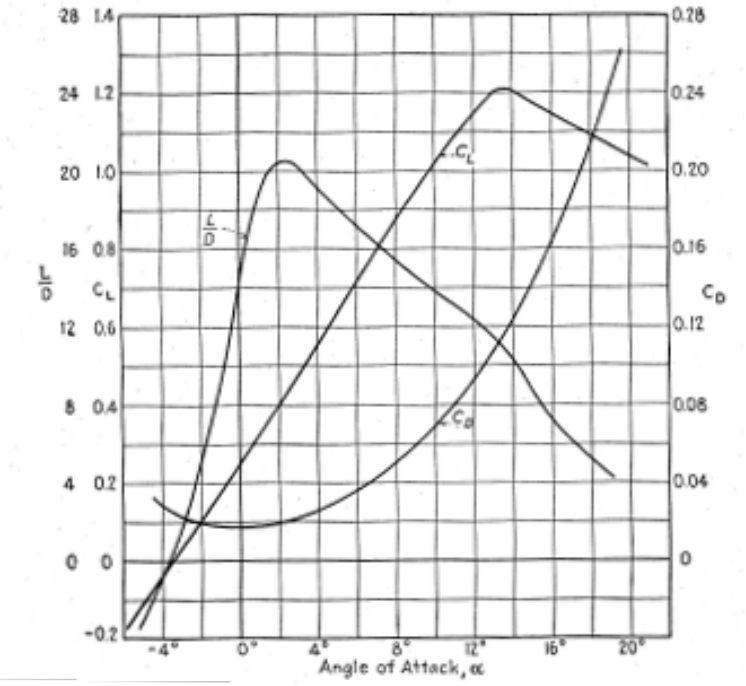


**Figure 23: Typical Coefficient of Lift and Drag Curve Chart [9].**

Comparing the optimized airfoil chart to the typical chart shows that the lift and drag curves match the expected shape for airfoil behaviors at various angles of attack.

To determine if improvements have been made on the propeller design, a baseline must be established from the existing propeller. As discussed previously, the data for the propellers are not available, so the propeller program would not be usable for calculating the efficiency. However, it is possible to estimate the efficiency from data from the thrust stand test. This estimation requires the current, voltage and RPM of the motor, as well as the thrust and radius of the propeller. The motor was running at 4750 RPM, with a thrust of 460 grams, a current of 5.14 Amps at a voltage of 11.3 V, and a propeller radius of 4.5 inches. Equation (79) provides the ideal power based on weight or thrust from the propeller, $W$ [34]. Thus,

$$Ideal\ Power = W * \sqrt{\frac{W}{2\rho A}}. \quad (79)$$

The ideal power must be converted to horsepower and then to watts. Using the watts going into the motor from testing, and assuming the motor efficiency of 80 percent, the propeller efficiency is obtained. Equation (80) shows the FOM for the ideal power to actual power, with motor efficiency:

$$FOM = \frac{Ideal\ Power}{Actual\ Power * Motor\ Efficieny}. \quad (80)$$

Using this estimate, the propeller efficiency is about 65 percent. The original goal was to reach at least 70 percent propeller efficiency. As this is higher than the current propeller, the goal remained the same.

Solving the propeller optimizer provided one hundred and forty-four solutions based on each airfoil being solved at four different diameters, 9, 10, 11, and 12 inches. The total range of efficiencies ranged from 47 percent to 83 percent. The results were sorted by highest efficiency and then by smallest tip theta. The smaller the tip theta, the lower the chance to have airfoil stalls along the blade. Table 5 shows the top ten solutions.

**Table 5: Propeller Data and Efficiencies.**

| AOA | Re | Theta | chord (m) | chord taper | Diameter (inches) | RPM | FOM |
|---|---|---|---|---|---|---|---|
| 4 | 100 | 6.5618 | 0.01 | 2 | 9 | 5500 | .8363 |
| 2 | 100 | 7.8614 | 0.01 | 1.5 | 9 | 5200 | .8339 |
| 3 | 318 | 7.9997 | 0.01 | 1.5 | 9 | 4700 | .8214 |
| 1 | 360 | 7.9997 | 0.02 | 1.5 | 9 | 5000 | .8134 |
| 4 | 100 | 3.9101 | 0.01 | 1.5 | 9 | 4700 | .812 |
| 2 | 100 | 4.6793 | 0.01 | 2 | 10 | 5100 | .8117 |
| 3 | 318 | 6.4147 | 0.01 | 1.5 | 10 | 4800 | .8093 |
| 1 | 360 | 7.5267 | 0.01 | 1.5 | 10 | 5400 | .8061 |
| 3 | 200 | 7.9997 | 0.02 | 1.5 | 9 | 4700 | .8015 |
| 2 | 218 | 7.9997 | 0.01 | 2 | 9 | 5200 | .7956 |

Based on the initial efficiency calculations, the goal has been met for achieving a better performing propeller than the stock propeller. The units in the table are mixed for the chord and the diameter, with the chord having an SI unit and the diameter having an English unit. This is done because the propellers are normally in English units and the chord length was set based on using a 3D printer, which is in SI units. The optimized airfoils for the range of Reynolds numbers each provided an optimized propeller with a FOM of above 80%. Overall, most of the lower Reynolds number airfoils performed at a lower FOM when comparing all of the designs. Despite this result, the top two performing designs were for the lowest Reynolds number airfoils. For most of the propellers, the chord length was made very small with a lower taper on the blade. The blade twist is normally high for the propellers, which is expected, because a higher blade twist increases the lift for the BEM theory. A noticeable exception to this is the fifth and sixth highest performing blades, as they have a fairly low blade twist. Without accounting for extra losses or uncertainties in the final propeller efficiencies, about one half of the designs performed at the baseline or better.

## Computational Fluid Dynamics (CFD) and Finite Element Analysis (FEA)

To verify the designs generated by the MATLAB program, two propellers were modeled in Solidworks to analyze in the CFD program, Flow Simulation. The CFD program allows the design to be tested against varying conditions to determine how it will react. It can provide information -- such as thrust, torque, pressure distribution, air streamline information, air velocities and other information -- based on the goals for the study. Adjusting the boundary conditions within the setup of the problem sets the varying

conditions for the analysis. These boundary conditions include the velocity of the airflow coming into the area of study, the environmental temperature and pressure, and the rotation of the body in space. Information calculated in the CFD program can also be used to provide the required loading to determine the stresses placed on the model during operation.

The two propellers chosen for this analysis were the angle of attack of 4 degrees at a Reynolds number of 100,000 and angle of attack of 1 degree at a Reynolds number of 360,000. Referring to Table 5, these designs consist of the highest FOM propeller and the fourth highest. The fourth highest was chosen for the second design because it was operating at a different Reynolds number, a different RPM, and a different chord length from the highest performing propeller. By studying these two very different propellers, it provided a greater opportunity to verify that the program generated multiple working solutions, which provides a greater level of confidence in its accuracy.

To model each propeller, a section was added to the MATLAB program that would generate text files for the geometry of the airfoils moving along the length of the propeller. The chord length, the angle of attack and the distance along the blade are modified in the geometry of the airfoil in the text files. Solidworks has a tool to import text files that have an x, y, and z coordinate system. This allowed for a higher accuracy in importing each airfoil as opposed to manually changing the chord length and pitch for each section. Manually modeling the propeller could have increased the amount of error generated in the CFD analysis because it would not have been an exact representation of the theoretical model. The importing tool only covered the shape of the propeller blade. The tip, root and motor connection had to be added after the propeller blade was modeled. The motor

connection was copied from the existing stock propeller because it has a low effect on the propeller performance and it works with the existing motor. The root of the propeller was a continuation of the airfoil shape that was tapered into a connection to the motor connector. The tip consisted of the airfoil shape tapered into an ellipse; this helps to cut down on tip vortices. Figure 24 shows one of the propeller models prior to CFD and FEA analysis.

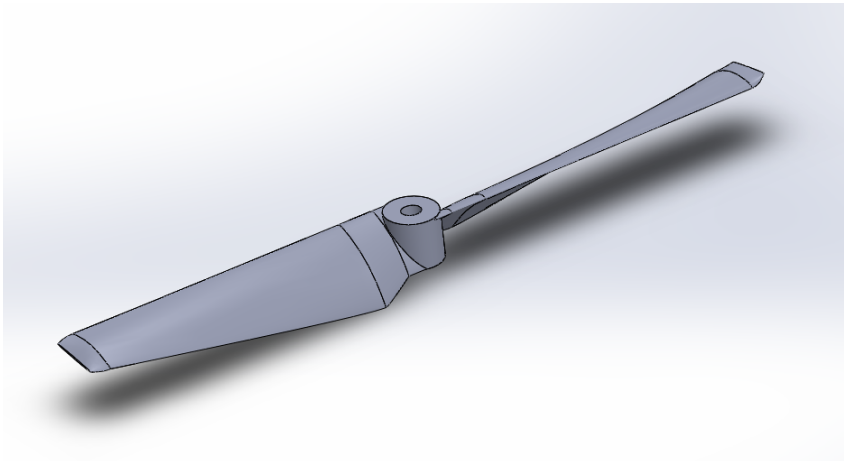

**Figure 24: Solidworks Propeller Model.**

To use the CFD method, the analysis needed to be set up to solve for the conditions the propeller will experience during normal operations. The environment was set to standard sea level temperature and pressure conditions. It is expected that the propeller will be subject to laminar and turbulent flows, so the built-in k-ε model combined with Van Driest's Two-Scale Wall Functions was used to solve for these flows [38]. The computational domain was set to at least two propeller diameters in the x-y plane and four propeller diameters in the z direction to ensure enough area was solved to fully develop the flow. A small flow was added to the system, .05 m/s, to assist the solver with the speed of the solution and to provide a better representation of the tip vortices development. The goals were set to determine the pressure across the propeller surfaces, the thrust and the

torque. The propeller motion was set to the RPM for each propeller, which was done by rotating a disk of air around the propeller. This step was needed because the CFD tool does not have any way to rotate the model in the computational space. Lastly, the analysis was run multiple times at increasing mesh densities to ensure the solutions were not affected. Figure 25 shows the mesh around the propeller. The high-density mesh occurs only near the propeller to capture the changes in geometry and how they affect the fluid cells. The low-density mesh can be used for the cells capturing smaller changes in fluid flow.

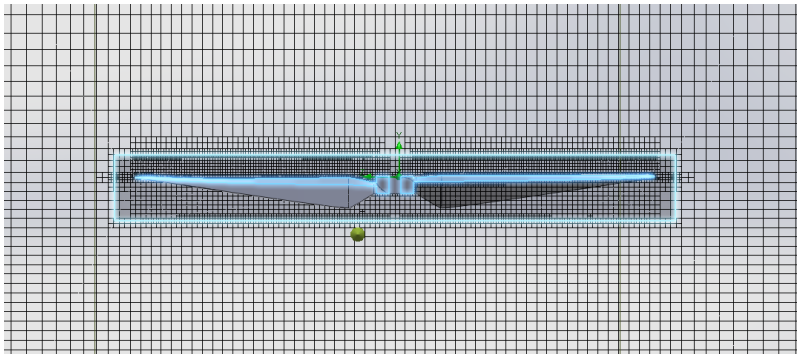

**Figure 25: Propeller Model Meshing.**

After the analysis was completed, the fluid flow lines were modeled to visually verify that the propeller was operating as expected. Figures 26 and 27 show different representations of the air streamlines.

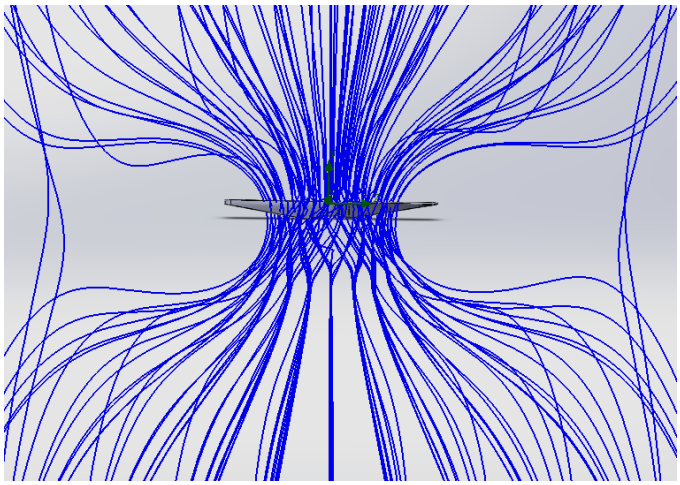

**Figure 26: 3D Air Streamlines Around the Propeller.**

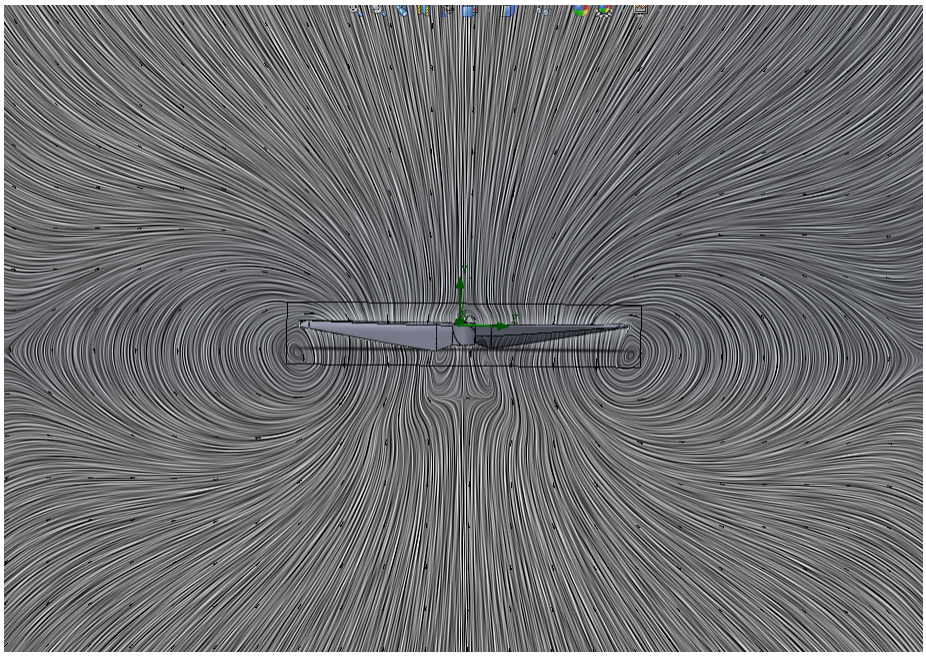

**Figure 27: 2D Air Streamlines Around the Propeller.**

As seen in Figure 27, most of the flows generated by the propeller occur from 35 to 75 percent of the blade, which is expected based on the propeller theory. From 75 percent of the blade to the tip, the airflow becomes a circular shape and has a very low component of thrust. This can also be seen to smaller effect near the root of the blade, but as this is where the propeller is connected to the motor, its effects are much smaller on the overall performance. Figure 26 shows the particles of air being brought into the propeller area and then leaving in a twisting pattern before moving back out to the steady straight streamlines. Figure 28 shows the pressure distribution along the blades. As expected, a low-pressure area forms over the top of the blades with a high-pressure area forming on the opposite bottom side, which generates lift for an airfoil or thrust for a propeller. The pressure distribution also closely matches what was seen in the streamline figures, in which the largest difference in pressure occurs in a range of about 40 to 80 percent of the propeller.

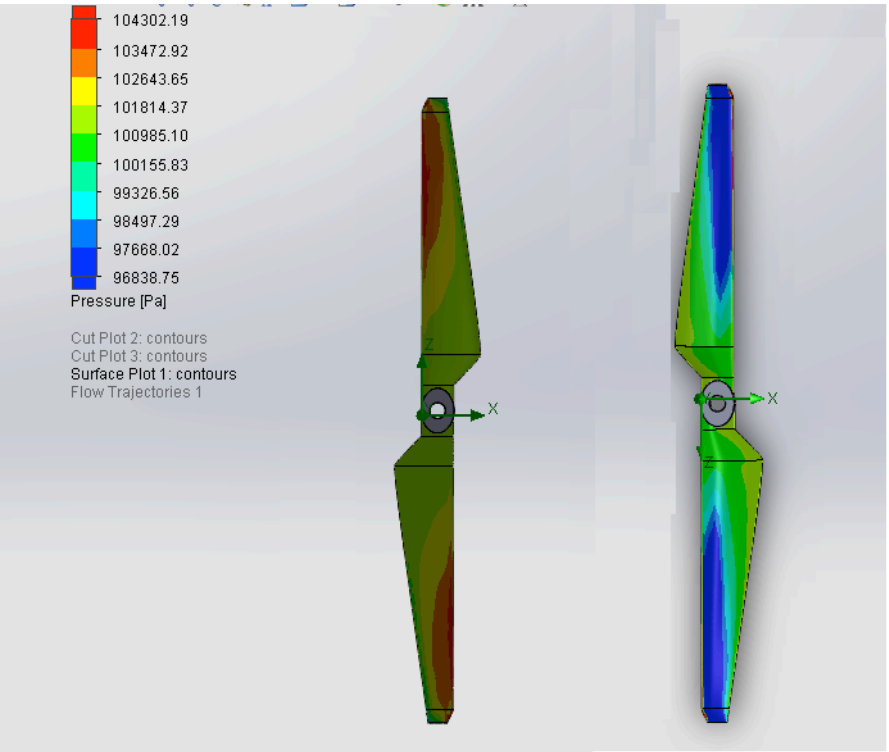


**Figure 28: Pressure Distribution on the Propeller.**

Table 6 shows the values obtained from the CFD analysis for each propeller design.

**Table 6: Propeller Data and Efficiencies from CFD Analysis.**

| AOA | Re | Thrust (N) | Torque (N*m) | FOM | Flight Condition |
|---|---|---|---|---|---|
| 4 | 100 | 4.489 | .086 | .83 | Hovering |
| 4 | 100 | 12.42 | .236 | .80 | Max Motor RPM |
| 1 | 360 | 4.24 | .091 | .81 | Hovering |
| 1 | 360 | 14.498 | .354 | .81 | Max Motor RPM |

Reviewing the data from Table 6 shows that the FOM of both propeller designs closely match what was theoretically calculated for hovering flight. The maximum motor RPM flight condition FOM is an estimate comparing the coefficient of thrust values versus the coefficient of power that closely matches the solving method for the hovering condition. For the CFD analysis, the flow conditions were kept at the same small amount as the hovering conditions to provide a comparison between the hovering state and maximum

motor RPM state. If the motors were operating at the maximum RPM, the generated thrust would cause the UAV to rise, thereby increasing the flow over the propeller. This flow condition would change how the propeller efficiency was calculated because it would then be based on forward flight instead of thrust versus torque. The thrust values generated by the propellers for both designs would be enough to keep the UAV hovering and provide adequate thrust for control and lift.

To ensure the propellers could withstand the forces applied to them while operating at the maximum motor RPM, the pressure results of the maximum motor RPM were imported into Solidworks Simulation to conduct a FEA analysis. The FEA analysis was set up to provide the stress values and their locations on the model, the deformation of the model, and the factor of safety. For the analysis, the propeller material was Nylon 6 with a 30 percent glass fill. The propeller was fixed to the motor shaft and placed on a slider where the bottom face of the propeller motor connection met the motor face. Figure 29 shows the meshing and fixtures for the model.

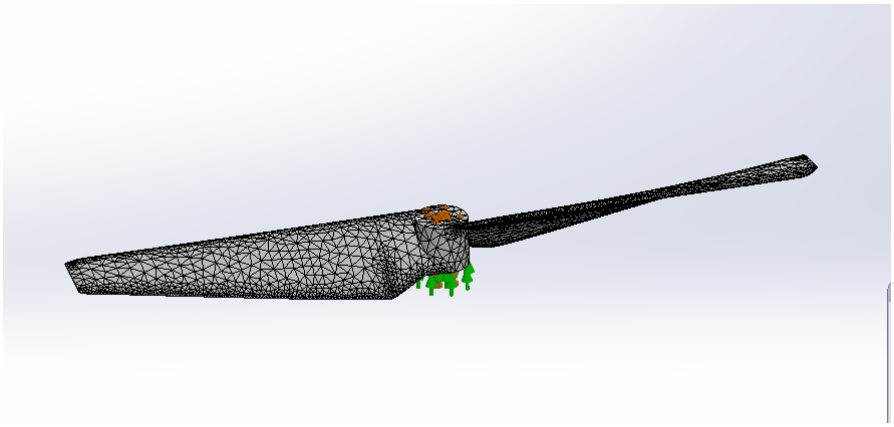

**Figure 29: Propeller Mesh and Fixtures for FEA Analysis.**

The first analysis conducted was on the 4-degree angle of attack propeller. Figure 30 shows the von Mises stresses as well as the maximum stress value and location.

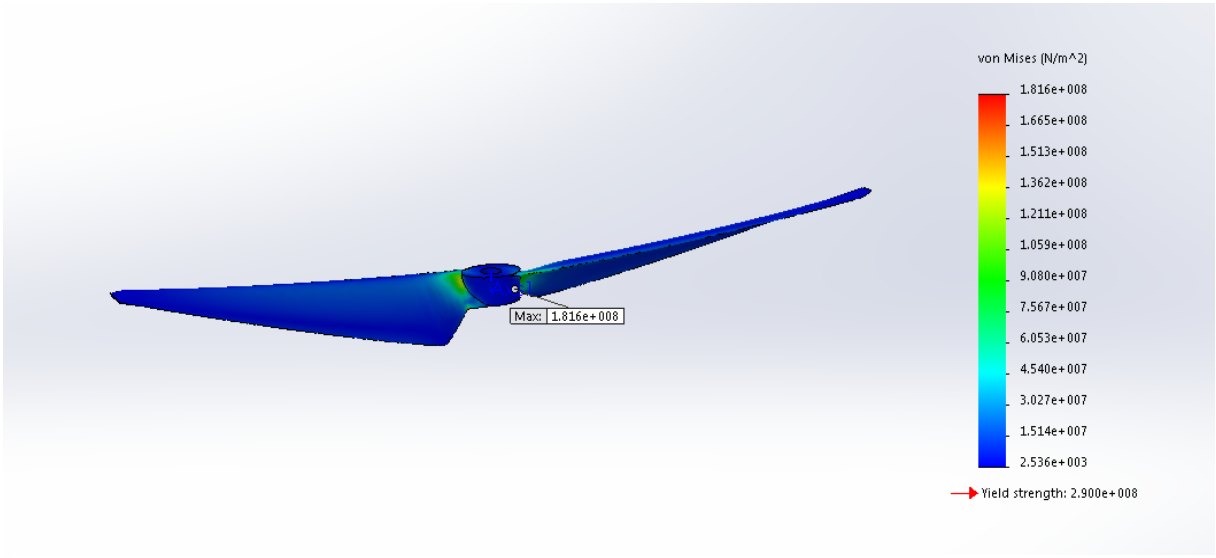


**Figure 30: Von Mises Stress on 4-Degree AOA Propeller.**

The maximum stress was 1.82 x $10^8$ N/$m^2$, which is located at the connection from the propeller to the motor connection hub. The yield strength of the material is 2.9 x $10^8$ N/$m^2$, meaning the stresses are well below the material level. Figure 31 shows the deformation of the propeller.

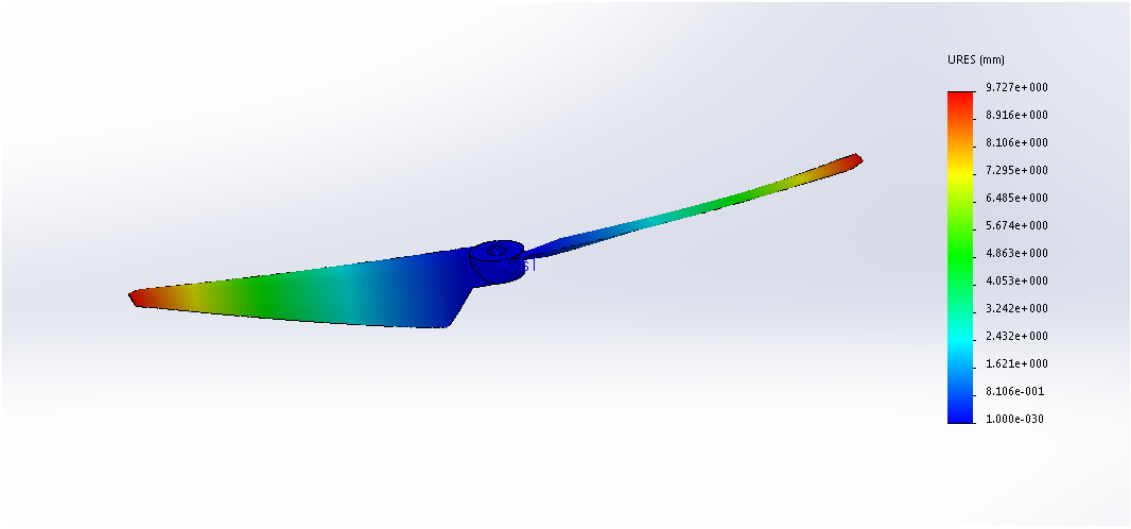


**Figure 31: Deformation on 4-Degree AOA Propeller.**

The maximum deformation occurs at the tips of the propeller and has a value of 9.73 mm. As the propeller blades are thin, a higher value of deformation is expected. Figure 32 shows the factor of safety.

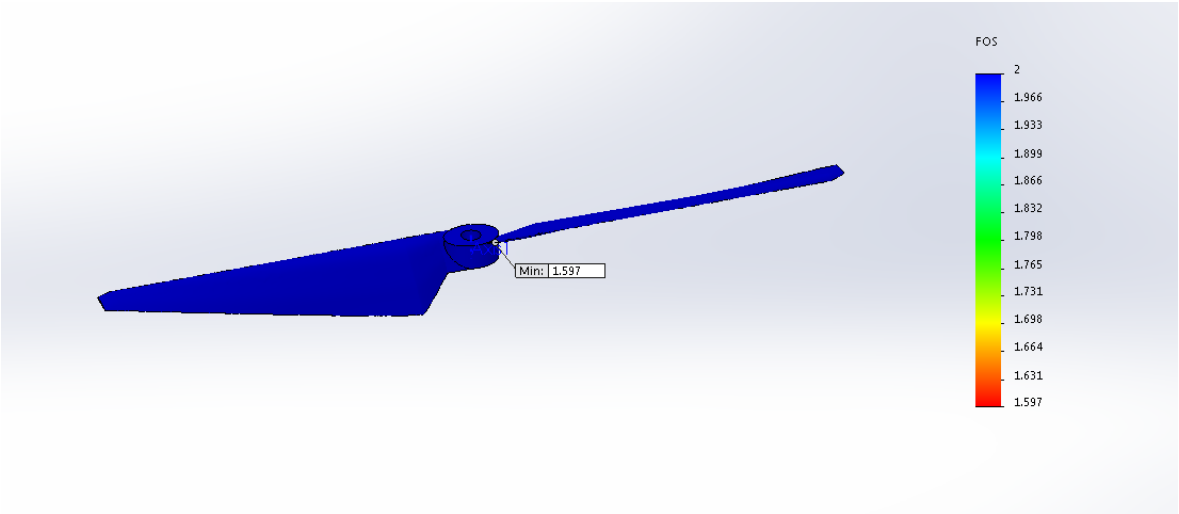


**Figure 32: Factor of Safety on 4-Degree AOA Propeller.**

The lowest factor of safety is 1.58 and occurs at the motor connection hub. The minimum specified value for the propeller factor of safety was 1.5. This propeller design meets the factor of safety requirements and has stresses below yield strength when operating at the maximum motor RPM.

This analysis was conducted on the second propeller design using the same connections and material properties. The pressure loading was updated to match the results from the corresponding CFD analysis. Figure 33 shows the Von Mises stresses on the second propeller.

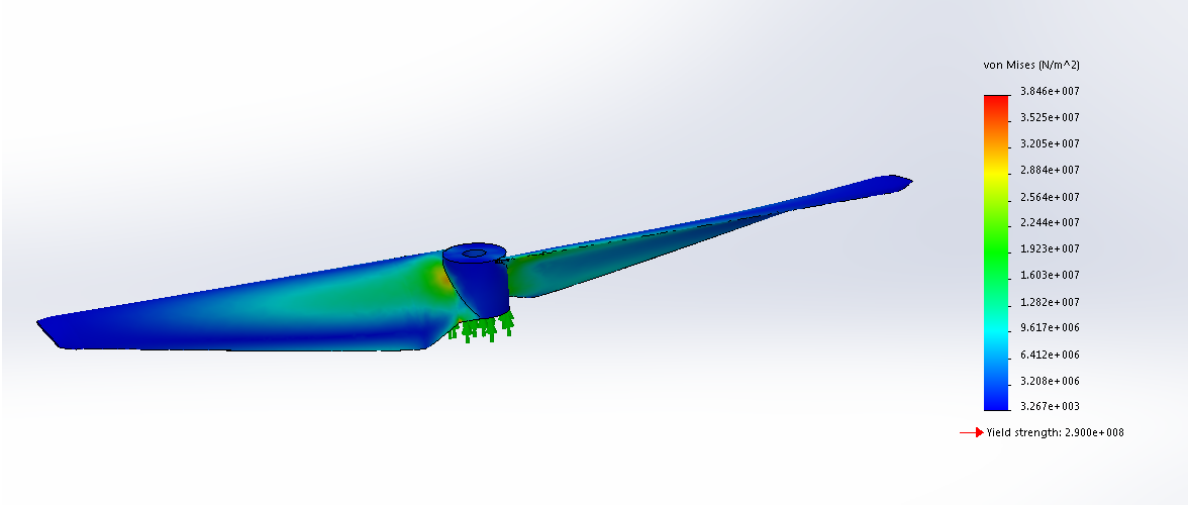


**Figure 33: Von Mises Stress on 1-Degree AOA Propeller.**

The maximum stress on the second propeller was 3.85 x $10^7$ N/$m^2$. It is located at the junction of the propeller blade and the taper to the root to motor connection. This high stress point appears to be caused by a sharp change in the angles of the trailing edge. The stresses are also much lower in the second propeller compared to the first because of the larger cross-sectional area of the blade. Figure 34 shows the deformation of the second propeller blade.

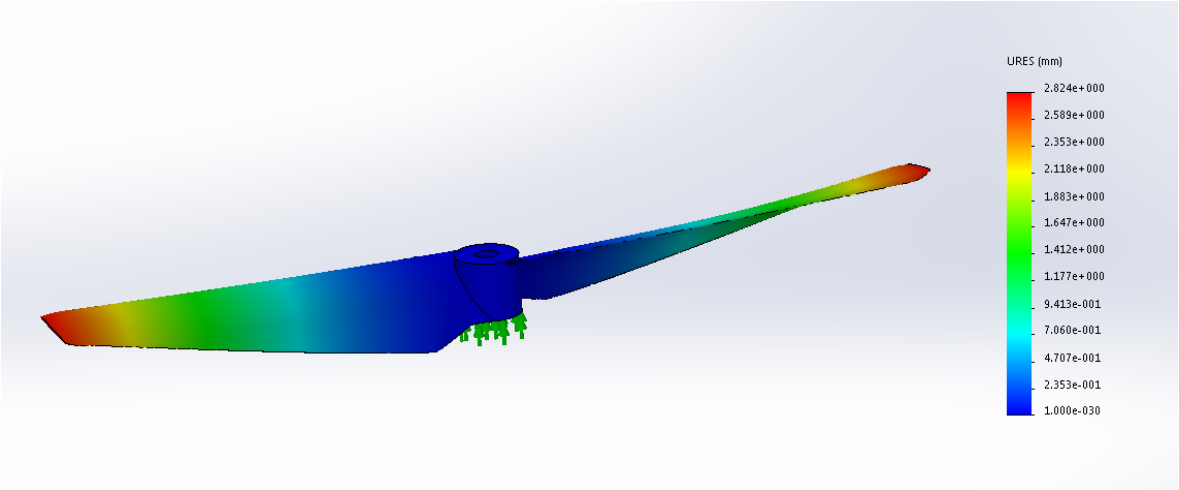


**Figure 34: Deformation on 1-Degree AOA Propeller.**

The maximum deformation for this propeller design is 2.82 mm. As seen with the Von Mises stresses, the deformation is much lower for this design. Figure 35 shows the

factor of safety for this propeller.

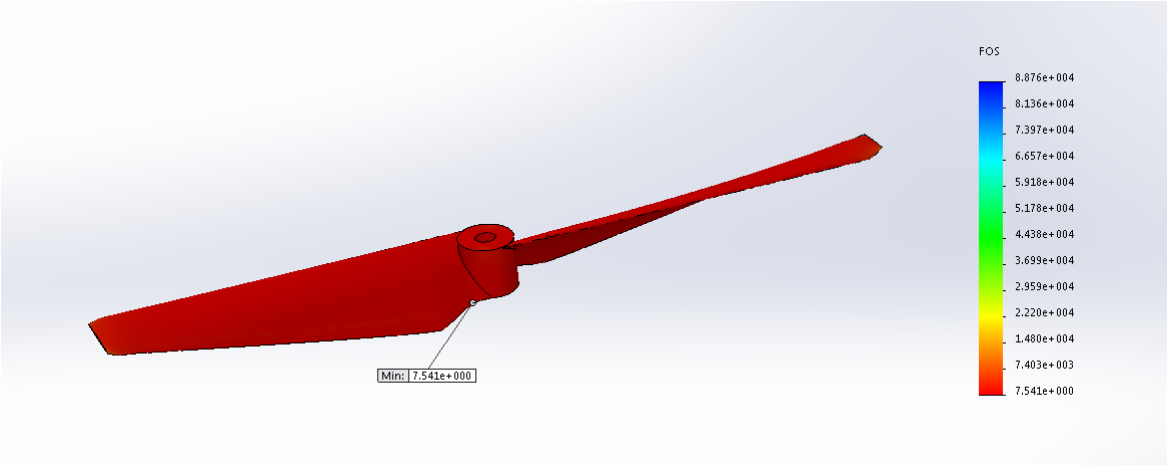


**Figure 35: Factor of Safety on 1-Degree AOA Propeller.**

The minimum factor of safety is 7.54 on this design and occurs at the high stress point seen in Figure 33. This propeller design meets the factor of safety requirement and is below the material yield stresses during maximum motor RPM operation.

## Conclusion and Recommendations

A method was developed to generate and test various airfoils and propellers through the use of a MATLAB program combined with Xfoil. This program used the CST method with $6^{th}$ order Bernstein Polynomials to generate airfoil shapes controlled by a hybrid pattern search particle swarm optimizer. The optimizer used Xfoil to generate the coefficients of lift and drag for each airfoil to obtain the best lift-to-drag ratio for four different Reynolds numbers over a range of angles of attack from 0 to 8 degrees. The MATLAB program was also used to generate propeller shapes using the modified BEM for hover equations. This was done by retrieving the airfoil lift and drag values and using them to determine the optimal chord length, chord taper, blade twist and motor RPM. The top two results from this program were modeled and tested in a CFD program to ensure that the results were accurate. These models were then tested in an FEA program to ensure they

would not mechanically fail during normal operations. Table 7 provides a summary of the results from the MATLAB program, the CFD analysis, and the FEA analysis.

**Table 7: Propeller Design Results Summary.**

| AOA | 4 | 4 | 1 | 1 |
|---|---|---|---|---|
| Re | 100 | 100 | 360 | 360 |
| Thrust (N) | 4.489 | 12.42 | 4.24 | 14.498 |
| Torque (N*m) | .086 | .236 | .091 | .354 |
| Flight Condition | Hover | Max RPM | Hover | Max RPM |
| MATLAB FOM | .8363 | - | .8134 | - |
| CFD FOM | .83 | .80 | .81 | .81 |
| Von Mises Stress ($N/m^2$) | - | $1.82*10^8$ | - | $3.85*10^7$ |
| Deformation (mm) | - | 9.73 | - | 2.82 |
| Factor of Safety | - | 1.59 | - | 7.54 |

The resulting FOM from the MATLAB program compared to the FOM from the CFD analysis is very close for both designs. This shows that the theoretical values obtained from the BEM equations can be expected to closely match the designed 3D model for performance. The thrust for both designs will be able to lift the UAV in a hovering state and provide enough lift to control the vehicle during flight. Both designs met the factor of safety requirement and did not have a higher stress than the material yield strength at the maximum motor RPMs. Lastly, both of the propeller designs had a higher efficiency than the baseline stock propeller. By verifying two different propeller designs, it was also shown that the program would be able to generate more efficient propellers for varying constrained variables. For example, if the manufacturing process required a certain thickness, chord length or twist, those types of variables could be set to a constant value and the program would still generate a more efficient design around that constraint. This flexibility will be helpful for adjusting the designs to maximize the performance around a motor's optimal

running conditions. Based on these results, the MATLAB program was able to generate designs that met all goals set for this project. The last recommended test for the code verification would be to manufacture the propeller designs and conduct wind tunnel testing. As the theoretical and CFD methods both have some error in their solutions, it would be helpful to test a physical model to determine if the program needs to be adjusted to account for these errors.

For continued work on this program, a couple of observations and features would be useful for improving the design method. During the airfoil optimization, Xfoil could provide unrealistic values of drag. It appears that this is caused by the $A$ coefficients reaching too many significant figures and causing geometry issues for Xfoil. This was tracked by viewing the objective function and corresponding $A$ values for the number of iterations. The optimizer would reach a reasonable solution but after a while of verifying the solution, the drag coefficient would drop significantly, providing numbers that were unusable. To help prevent this, the $A$ values were truncated in the optimizer to lessen the chance of this phenomenon occuring. As seen in the coefficient of lift and drag curves, some points are missing from the solution, which is due to Xfoil freezing on some geometries and varying angles of attack. This is a known issue in Xfoil but no solutions were offered in the help section to alleviate this problem. To allow the MATLAB program to continue to solve with this issue, coding was added to ignore this error and to skip it in the solution. This procedure did not affect the overall lift or drag curves, as enough points were determined to generate the required data. Because of these Xfoil issues, it may be worthwhile to spend time developing a panel method that could accept a wider range of geometries and angles of attack without crashing. A new panel method would also help to

alleviate the reduced drag coefficients at certain significant figure geometries. Other features that would improve the usefulness of the program include adding propeller optimization around motor efficiency curves, blended airfoil propeller blades, and forward flight optimization. The optimization for motor curves would help to ensure the propeller operates at an optimal level while running the motor at its most efficient level. This would greatly improve battery life by reducing the lost current while operating the motor in the lower efficiency portion of the motor performance curve. The blended airfoil method would use the best-suited optimized airfoil for different sections along the blade. As the angle of attack and Reynolds number change along the length of the propeller blade, this approach would use the airfoil with the best lift-to-drag coefficient for each section based on those changing values. The forward flight optimization could be an addition used for many applications, such as better overall performing propellers for multicopter aircraft or propellers for fixed wing types of UAVs. Adding this feature to the propeller optimization would allow the program to generate a propeller that was optimized for both hovering conditions and higher thrust moving conditions. As these two conditions can be conflicting for optimization, each condition could be weighted based on the desired flight characteristic for the UAV.

# References


[1] Aerospace Industries Association. 10 May 2013. "Unmanned Aircraft Systems: Perceptions & Potential". PDF Report from AIA. [Internet, WWW, PDF]. *Available*: Available in .PDF format from Aerospace Industries Association; Address:http://www.aiaaerospace.org/research_reports/unmanned_aircraft_systems_perceptions_and_potential/ [Accessed: 15 October 2015]. A copy is available from the company's website.

[2] Center for a New American Security. June 2015. "A World of Proliferated Drones: A Technology Primer". PDF Paper from Center for a New American Security. [Internet, WWW, PDF]. Available from Center for a New American Security. Address: http://www.cnas.org/research/world-of-proliferated-drones [Accessed: 16 October 2015]. A copy is available from the group's website.

[3] Kleinman, Zoe. 8 January 2015. "CES 2015: Why the Future of Drones is Up in the Air". From BBC News. [Internet, WWW]. Available from the BBC News Website. Address: http://www.bbc.com/news/technology-30721339. [Accessed: 16 October 2015]. A copy of the article is available from the website.

[4] Gonzalez, Santiago. 11 January 2015. "The Future of Drones – 2015 International Consumer Electronics Show". From The Speaker 21st Century News. [Internet, WWW]. Available from the Speaker News Website. Address: http://thespeaker.co/technology/future-drones-2015-international-consumer-electronics-show/. [Accessed: 12 November 2015]. A copy of this article is available from the website.

[5] HobbyKing. 10 November 2015. Batteries and Accessories. Current range of battery technologies available is shown. From HobbyKing store website. [Internet. WWW]Address:http://www.hobbyking.com/hobbyking/store/__86__85__Batteries_Accessories-Li_Poly_All_brands_.html. [Accessed: 16 October 2015]. The website provides current battery options.

[6] Higgins, George J. May 1925. "The Comparison of Well Known and New Wing Sections Tested in the Variable Density Wind Tunnel." Technical Notes National Advisory Committee for Aeronautics NO. 219. [Internet, WWW, PDF]. Langley Memorial Aeronautical Laboratory. Available from NASA Technical Reports Server. Address: http://ntrs.nasa.gov/search.jsp?R=19930081027. [Accessed: 15 October 2015]. A copy is available from the website.

[7] Weick, Fred. May 1926. *Propeller Design – Practical Application of the Blade Element Theory – I.* No. 235. From National Advisory Committee for Aeronautics. [Internet, WWW, PDF]. Langley Memorial Aeronautical Laboratory. Available from NASA Technical Reports Server. Address:

http://ntrs.nasa.gov/search.jsp?R=19930081014. [Accessed: 15 October 2015]. A copy is available from the website.

[8] Durand, William. January 1920. *Experimental Research on Air Propellers.* NACA-TR-14. From National Advisory Committee for Aeronautics. [Internet, WWW, PDF]. *Available*: Available from NASA Technical Reports Server. Address: http://naca.larc.nasa.gov/search.jsp?R=19930091058&qs=Ns%3DPublication-Date%7C0%26N%3D4294966056%26Nn%3D4294730567%257CNASA-Center%257CStennis%2BSpace%2BCenter. [Accessed: 15 October 2015]. A copy is available from the website.

[9] Weick, Fred. 1930. *Aircraft Propeller Design.* McGraw-Hill Book Company. The Maple Press Company, York, PA.

[10] APCPROP.com. 10 November 2015. Existing Propellers for UAV and MAVs. From APC store website. [Internet. WWW]. Address: http://www.apcprop.com/pindex.asp?Page=2. [Accessed: 10 October 2015]. The website provide current propeller options.

[11] Merchant, Monal. 2004. "Propeller Performance Measurement for Low Reynolds Number Unmanned Aerial Vehicle Applications." Master's Thesis, from Wichita State University. [Internet, WWW, PDF]. Available from Wichita State University website-SOAR.Address: soar.wichita.edu/xmlui/bitstream/handle/10057/773/t05031.pdf. [Accessed: 15 October 2015]. A copy is available from the university website.

[12] Brandt, John. Selig, Michael. January 2011. "Propeller Performance Data at Low Reynolds Numbers." 49th AIAA Aerospace Sciences Meeting. 4-7 January 2011. From the University of Illinois at Urbana-Champaign. [Internet, WWW, PDF] *Available:* Available from the university's website. Address: http://m-selig.ae.illinois.edu/pubs/BrandtSelig-2011-AIAA-2011-1255-LRN-Propellers.pdf. [Accessed: 16 October 2015]. Available from University of Illinois at Urbana-Champaign website.

[13] Anderson, John D. 2011. *Fundamentals of Aerodynamics.* 5th. Ed. McGraw-Hill Companies, INC. Avenue of the Americas, New York, NY.

[14] Boucher, Robert J .1994. *The Electric Motor Handbook: The Complete Handbook of High Performance D.C Motors*. 2nd Ed. Astroflight.

[15] Harbaug, Arlen. 13 June 2007. "Designing an Electric Power System for an R/C Plane." PDF paper from Loudoun County Aeromodelers Association (LCAA). [Internet, WWW, PDF]. *Available*: Available in .PDF format from LCAA website. Address: http://www.lcaa.org/pdf/electric_power_design_2.pdf. [Accessed 15 October 2015]. A copy is available from the association's website.

[16] Kulfan, Brenda. February 2008. "Universal Parametric Geometry Representation Method." *Journal of Aircraft*. Vol. 45, No. 1, January-February 2008. *Available*: Available from Brenda Kulfan. [Internet, WWW, PDF]. Address: http://smtp.brendakulfan.com/docs/CST6.pdf [Accessed: 28 November 2015]. A copy is available from the website.

[17] Drela, Mark. 11 December 2000. *Xfoil Subsonic Airfoil Development System* (Version 6.99). [Internet, WWW, Computer Program] *Available*: Available from Massachusetts Institute of Technology website. Address: http://web.mit.edu/drela/Public/web/xfoil/. [Accessed: October 12, 2015]. A copy of the software is available from the website.

[18] Carmichael, B. H. NASA. 1 November 1981. *Low Reynolds Number Airfoil Survey.* Report No. 165803. From NASA contractor report. [Internet, WWW, PDF]. *Available*: Available from NASA Technical Reports Server. Address: http://ntrs.nasa.gov/search.jsp?R=19820006186. [Accessed 10 October 2015]. A PDF copy is available from the website.

[19] Rutkay, Brian. 2014. "A Process for the Design and Manufacture of Propellers for Small Unmanned Aerial Vehicles". Master's Thesis. From Carleton University. [Internet, WWW, PDF]. *Available*: Available from Carleton University Research Virtual Environment. Address: https://curve.carleton.ca/9e14f851-773a-4174-af17-70beb6f6c7a7. [Accessed: 14 October 2015]. A copy is available from the university website.

[20] McCrink, Matthew. Gregory, James. June 2015. "Blade Element Momentum Modeling of Low-Re Small UAS Electric Propulsion Systems". 33rd AIAA Applied Aerodynamics Conference 22-26 June 2015. From Ohio State University. *Available*: Available from The American Institute of Aeronautics and Astronautics. [Internet, WWW, PDF]. Address: http://arc.aiaa.org/doi/abs/10.2514/6.2015-3296. [Accessed: 14 October 2015]. A copy is available from the website.

[21] Prathapanayaka, R. Kumar, Vinod. Kumar, Santhosh. Krishnamurthy, S.J. Sharma, Narendra. February 2015. "Realist Assessment of Efficiencies of Mirco Air Vehicle Propellers". *From International Journal of Innovative Research in Science, Engineering and Technology*. Vol. 4, Issue 2, February 2015. *Available*: Available from International Journal of Innovative Research in Science, Engineering and Technology website. [Internet, WWW, PDF]. Address: http://www.ijirset.com/upload/2015/february/31_7_Realistic.pdf. [Accessed: 15 October 2015]. A copy is available from the website.

[22] Leishman, Gordon. April 2006. *Principles of Helicopter Aerodynamics*. 2nd, Ed. Cambridge University Press.

[23] Smedresman, Adam. Yeo, Derrick. Shyy, Wei. June 2011. "Design, Fabrication, Analysis and Testing of a Micro Air Vehicle Propeller." 29th AIAA Applied Aerodynamics conference 27-30 June 2011. From the University of Michigan, Ann Arbor. [Internet, WWW, PDF]. *Available*: Available from the AIAA website. Address: http://arc.aiaa.org/doi/abs/10.2514/6.2011-3817. [Accessed 12 October 2015]. A PDF copy is available from the AIAA website.

[24] Wall, David. 2012. 4 August 2012. "Optimum Propeller Design for Electric UAV's". Master's Thesis, from Auburn University. [Internet, WWW, PDF]. Available from the University of Auburn, Alabama website. Address: https://etd.auburn.edu/bitstream/handle/10415/3158/David_Wall_Thesis.pdf?sequence=2. [Accessed 13 October 2015]. A PDF copy is available from the University of Auburn, Alabama website.

[25] Dr. Hepperle, Martin. 1996. PropellerScanner (Version1.1). [Internet, WWW, Computer Program]. *Available*: Available from aerotools website. Address: http://www.mh-aerotools.de/airfoils/software.htm. [Accessed 12 October 2015].

[26] Deters, Robert. Ananda, Gavin. Selig, Michael. June 2014. "Reynolds Number Effects on the Performance of Small-Scale Propellers". 32nd AIAA Applied Aerodynamics Conference 16-20 June 2014. From the University of Illinois at Urbana-Champaign. [Internet, WWW, PDF]. *Available*: Available from the university's website. Address:http://m-selig.ae.illinois.edu/pubs/DetersAnandaSelig-2014-AIAA-2014-2151.pdf. [Accessed 15 October 2015]. A PDF copy is available from the website.

[27] NASA History Program Office. 10 November 2015. Provides information on the history of NASA. From National Aeronautics and Space Administration website. [Internet, WWW]. Address: http://history.nasa.gov/naca/. [Accessed 10 November 2015].

[28] Aerospaceweb. "NACA 4-Digit Airfoil Equations". Article from Aerospaceweb. [Internet, WWW]. *Available*: Available from Aerospaceweb.org. Address: http://www.aerospaceweb.org/question/airfoils/q0100.shtml [Accessed: 30 December 2015]. A copy is available on the website.

[29] Abbott, Ira H. Doenhoff Albert E. and Stivers Jr, Louis S. " Summary of Airfoil Data." Report Number 824. From National Advisory Committee for Aeronautics. [Internet, WWW, PDF]. *Available*: Available from Nasa Technical Reports Server. Address: http://ntrs.nasa.gov/archive/nasa/casi.ntrs.nasa.gov/19930090976.pdf [Accessed: 30 December 2015]. A copy is available from the website.

[30] Unversity of Clarkston. "The NACA Airfoil Series." Article from Univeristy of Clarkston. [Internet, WWW, PDF] *Available*: Available from the University of Clarkston website. Address:

http://people.clarkson.edu/~pmarzocc/AE429/The%20NACA%20airfoil%20series.pdf [Accessed 30 December 2015]. A copy is available from the website.

[31] Joy, Kenneth I. "On-Line Geometric Modeling Notes: Bernstein Polynomials". Department of Computer Science, University of California, Davis. [Internet, WWW, PDF]. Available from University of Davis website. Address: http://www.idav.ucdavis.edu/education/CAGDNotes/Bernstein-Polynomials.pdf [Accessed 2 December 2015]. A PDF copy is available from the UC Davis website.

[32] Casselman, Bill. "From Bezier to Bernstein" Article from American Mathematical Society. [Internet, WWW]. *Available*: Available from the American Mathematical Society website. Address: http://www.ams.org/samplings/feature-column/fcarc-bezier [Accessed on 2 December 2015]. A copy is available from the website.

[33] Seddon, J. 1990. *Basic Helicopter Aerodynamics*. BSP Professional Books. Oxfod London Edinburgh Boston Melbourne

[34] Leishman, Gordon. 2006. *Principles of Helicopter Aerodynamics*. 2nd Ed. Cambridge University Press.

[35] Kanput IIT. 8 July 2012. "Introduction to Helicopter Aerodynamics and Dynamics." Presentations 4 through 7 at NPTEL. [Internet, WWW, PDF]. *Available*: From NPTEL website. Address: http://nptel.ac.in/courses/101104017/ . [Accessed: 5 January 2016]. The lectures are available from the website.

[36] 3drobotics. 2014. Iris+ Model Photos. Photo showing the current design of MAV. From 3Drobotics website. [Internet, WWW, Photo]. Address: https://store.3drobotics.com/products/iris. [Accessed on 15 October 2015]. The website provides general information and photos about the MAV.

[37] Perez, J.R and Basterrechea, J. 2009. "Hybrid Particle Swarm-Based Algorithms and their Application to Linear Array Synthesis". Department of Communications Engineering, University of Cantabria. [Internet, WWW, PDF]. Available from Progress in Electromagnetics Reaserach, PIER. Address: http://www.jpier.org/PIER/pier90/05.08122212.pdf [Accessed 20 December 2015]. A PDF copy is available from the PIER website.

[38] Hawkridge Systems. "Enhanced Turbulence Modeling in Solidworks Flow Simulation". Technical Paper from Hawkridge Systems. [Internet, WWW, PDF]. *Available*: Available from Hawkridge Systems.com. Address: http://www.hawkridgesys.com/file/solidworks-flow-simulation/enhanced-turbulence-modeling.pdf [Accessed: 17 April 2016]. A copy is available on the website.

# Bibliography

Aerospace Industries Association. May 2013. "Unmanned Aircraft – Unmatched Potential". Photo from Aerospace Industries Association website. [Internet, WWW, Photo]. *Available*: Available in photo format from Aerospace Industries Association; Address:.http://www.aiaaerospace.org/news/civil_unmanned_aircraft_systems_uas/ [Accessed: 15 October 2015]. A copy is available from the company's website.

Academy of Model Aeronautics (AMA). 10 November 2015. Provides insurance, training and rules for operation of all model aircraft. [Internet, WWW]. Address: http://www.modelaircraft.org/documents.aspx. [Accessed on 10 November 2015]. Available PDFs and webpages provide rules for safe operation of model aircraft.

Anwar, Muhammad. Ikramullah, Shahid. Mazhar, Farrukh. 2014. "Reverse Engineering in Modeling of Aircraft Propeller Blade – First Step to Product Optimization". *IIUM Engineering Journal*, Vol. 15, No. 2, 2014. PDF article from IIUM Engineering Journal. [Internet, WWW, PDF]. *Available*: Available from IIUM Engineering Journal website. Address: http://journals.iium.edu.my/ejournal/index.php/iiumej/article/viewFile/497/406. [Accessed 11 October 2015]. A copy is available from the journal's website.

Bedell, Frederick. 1919. *The Air Propeller*. D. Van Nostrand Company. 25 Park Place, New York.

Circiu, Ionica. Pahonie, Radu. Boscoianu, Mircea. "Considerations About the Micro Propeller Design and it's Integration with the Aerodynamic Surfaces". *Technical Sciences and Applied Mathematics*. PDF from Henri Coanda Air Force Academy. [Internet, WWW, PDF]. *Available*: Available from AFAHC website. Address: http://www.afahc.ro/ro/revista/Nr_1_2009/Art_Circiu.pdf. [Accessed 12 October 2015. A copy is available from the Henri Coanda Air Force Academy.

CNBC. 13 May 2015. *Here's Where the Real Money is in Drones*. Article from CNBC website. [Internet, WWW]. *Available*: Available from the CNBC website. Address: http://www.cnbc.com/2015/05/13/heres-where-the-real-money-is-in-drones.html. [Accessed on 15 October 2015]. A copy is available from the website.

DreeseCode Software LLC. *DesignFOIL* (Version 6). [Internet, WWW, Computer Program]. *Available*: Available from the company's website. Address: http://www.dreesecode.com/designfoil/index.html. [Accessed 12, October 2015]. A copy is available for purchase from the company's website.

Federal Aviation Administration (FAA). 10 November 2015. Provides rules, regulations and information on safely flying all types of aircraft. From Federal Aviation Administration website. [Internet, WWW]. Address: https://www.faa.gov/uas/. [Accessed 10 November 2015]. Current rules and classifications for UAV flights are shown on this website.

Forbes. 7 May 2015. *Drone Overlord Frank Wang On DJI's Milestones, Miscarried GoPro Partnership & Corporate Espionage*. Article from Forbes, Business website. [Internet, WWW]. *Available*: Available from the Forbes website. Address: http://www.forbes.com/sites/forbesasia/2015/05/07/drone-overlord-frank-wang-on-djis-milestones-miscarried-gopro-partnership-corporate-espionage/. [Accessed on 15 October 2015]. A copy is available from the website.

Garner, W. B. 2009. March 2009. "Model Airplane Propellers". PDF from DC Radio Control Club. [Internet, WWW, PDF]. *Available*: Available from DCRC website. Address: http://www.dc-rc.org/pdf/Model%20Propellers%20Article.pdf. [Accessed 12 October 2015]. A PDF copy is available from the DCRC website.

Heene, Mario. 2012. "Aerodynamic Propeller Model for Load Analysis" Master's Thesis. University of Stockholm, Sweden. From Royal Institute of Technology. [Internet, WWW, PDF]. *Available*: Available from DiVA institutional repository for research publications. Address: http://www.diva-portal.org/smash/get/diva2:559083/FULLTEXT01.pdf. [Accessed 12 October 2015]. A PDF copy is available from the DiVA website.

IBISWorld. April 2015. "IBISWorld Industry Report OD4424. Unmanned Aerial Vehicle (UAV) Manufacturing in the US." From IBISWorld website. *Available:* Available from IBISWorld website by purchasing. [Internet, WWW, PDF] Address: https://www.ibisworld.com/industry/unmanned-aerial-vehicle-uav-manufacturing.html. [Accessed on 11 November 2015]. A copy is available from the website.

Nelson, Wilbur. 1944. *Airplane Propeller Principles.* John Wiley and Sons, INC. Chapman and Hall, LTD. London.

Parrot Drone. 10 November 2015. A drone company that makes easy to control, user-friendly drones. From Parrot Drone company's website. [Internet, WWW]. Address: http://ardrone2.parrot.com. [Accessed 10 November 2015]. The website provides information on the company's drones.

Spoerry, T. Dr. Wong, K.C. 2006. "Design and Development of a Micro Air Vehicle Concept: Project Bindle". PDF from the School of Aerospace, Mechanical and Mechatronic Engineering, University of Sydney. [Internet, WWW, PDF]. *Available*: Available from the University of Sydney. Address: http://www.aeromech.usyd.edu.au/wwwuav/papers/Paper_mAV_Bidule.pdf. [Accessed 12 October 2015]. A PDF is copy available from the University of Sydney website.

Visiongain. 5 January 2015. "Small Unmanned Aerial Vehicle (UAV) Market Forecast 2015-2016". PDF report from Visiongain. [Internet, WWW, PDF]. *Available*: Available .PDF sample for free, full report requires purchasing. Address: https://www.visiongain.com/Report/1437/Small-Unmanned-Aerial-Vehicle-(UAV)-Market-Forecast-2015-2025. [Accessed: 15 October 2016]. A copy is available from the website.

Weick, Fred. December 1960. “Design and Build Your Own Propeller”. EAA No. 7882. PDF from Experimental Aircraft Association (EAA) archives. [Internet, WWW, PDF]. *Available*: PDF available from the EAA archives website with membership. Address: http://www.eaa.org/eaa/aviation-education-and-resources/eaa-magazines-and-publications/eaa-sport-aviation-magazine/sport-aviation-archive. [Accessed 14 October 2015]. A copy is available from the website.

# Appendix A: MATLAB Program Description

This section provides a walkthrough of the MATLAB code used to generate the propellers that were invetigated in this report. The MATLAB code was developed on the 2015b version of the software. The analysis was completed using a Macbook Pro and a MSI G60 Ghost Pro. Because of the size and complexity of the program, it was divided into sections that were devoted to solving a single part of the analysis. These sections included: the main program, airfoil optimizer, class shape, Xfoil interface, call back function, propeller optimizer, Lagrangian cubic interpolation, fminsearch with boundaries, and BEMT.

The main program serves as the user interface for operating the program. This program has five subsections that generate different data sets for future use or output data for the airfoil and propeller design. All of the subsections require the user to input the Reynolds number, Mach number, and the range of the angles of attack for the desired design optimization. These variables are carried through each subsection by assigning them as global variables. The user must also select which subsection to run based on the current phase of the design process.

The first subsection generates the optimized airfoils by calling the subprogram or function airfoil optimizer. This function requires the number of variables to be used in the CST method, fourteen for this design, a set of initial values to be used to start the optimizer, and the lower and upper boundaries for each variable. The airfoil optimizer changes the fourteen variables while searching for the best lift-to-drag ratio for each airfoil. This is done by using the internal MATLAB pattern search and particle swarm functions. The first step of the airfoil optimizer is to run the call back function. This function starts a timer each optimization cycle to determine if the program has failed to solve for the current

airfoil geometry. This timer limit can be adjusted by the user to provide more time for a less powerful computer and shorten it for a faster computer. The lower time setting will allow for the optimization to be reached at a quicker rate, provided that a majority of the airfoils provide solutions. If the timer is set to too short of a time for a slow computer, it may not reach an optimized solution. This call back function will also allow the program to continue to run in the event of an Xfoil geometry failure. This is caused by Xfoil crashing or freezing on certain geometries. The call back function will force shutdown of the Xfoil program and cause the optimizer to generate a new set of geometry variables. The second function, class shape, uses the fourteen geometry variables to generate the x and y coordinates for the airfoil, which is done by using the CST method described in the report. These coordinates are passed along to the Xfoil interface function. This function uses the Reynolds number, Mach number, angle of the attack, and the coordinates to create a dat file with instructions to run Xfoil and then obtain the results. The results are passed back into the airfoil optimizer, which checks it against previous solutions to search for the optimal result. When the optimal results are achieved, the results are sent back to the main program. These results include the fourteen geometry variables, the lift and drag coefficients, the angle of attack and the Reynolds number. The main program generates a text file based on this information for future use. This program will repeat until all of the Reynolds numbers, Mach numbers and angle of attack combinations have been solved, which will then end the program.

The second subsection uses the text file data from the first section to generate data points for the lift and drag curves for each airfoil over the range of angles of attack. The program starts by initializing the call back function, which is used in the same fashion as the first

subprogram. If Xfoil fails to provide a solution or freezes, it will allow the program to continue with the next values. The program then reads the fourteen geometry variables and uses the class shape function to regenerate the x and y coordinate points. This is passed along to the Xfoil function, along with a range of angles of attack to analyze the airfoil at. The lift and drag coefficients are created for the airfoil for each angle of attack. This information is output in a text file using the Reynolds number and initial angle of attack as an identifier.

The third subsection uses the curves generated from the second section to generate the propeller blade information. This section calls the propeller optimizer function, and passes the Reynolds number and initial airfoil angle of attacks into it. The propeller optimizer then reads the text files to obtain the lift and drag coefficients for each airfoil. These data are prepared from the optimizer function by creating two linear data arrays for the lift coefficient and by using a Lagrangian cubic interpolation function for the drag coefficients. This had to be done to fill in the holes in the data caused by Xfoil errors. This information is run through the fminsearch with boundaries function, which changes the propeller radius, RPM, blade taper ratio and the tip chord length while searching for the highest FOM. The user can set the boundary conditions for this optimizer to prevent a solution that is unusable for the design requirements, such as a limitation on the maximum radius. The fminsearch with boundaries function calls the BEMT function, which generates the FOM for each airfoil and propeller blade combination. The BEMT function uses the modified lift and drag coefficient data, the propeller radius, the RPM, the tip chord length, the blade taper and the aircraft weight to guess the initial propeller shape. This shape is used to generate the coefficient of thrust that is tested against the minimum coefficient of thrust. If the

values do not match, the propeller is modified until it reaches a value within the tolerance level of the required thrust coefficient. The coefficient of torque is then generated for this propeller to determine the FOM. This process is repeated until the highest FOM for each airfoil and propeller combination is determined. Text files are generated with the results including all of the propeller design information.

The fourth and fifth subsections of the main program generates the airfoil shapes to be imported into Solidworks and Solidworks CFD. This is done reading the text files generated by the third subsection and using the data to reconstruct the propeller and airfoil shape. Four slices of the propeller blade are taken at different points, 20 percent, 75 percent, the tip, and the root connection. These slices are exported into their respective coordinate systems based on the shape of the airfoil and the angle of attack from the propeller twist. These slices are exported to a text file format that can be imported into Solidworks for modeling.

**Engineering**

**Capstone Report Approval Form**

**Master of Science in Engineering – MSE**

**Milwaukee School of Engineering**

This capstone report, titled "Analysis and Design of a Low Reynolds Propeller for Optimal Unmanned Aerial Vehicle (UAV) Flight," submitted by the student Alan Mushynski, has been approved by the following committee:

Faculty Advisor: _____ Date: _____

Dr. Subha Kumpaty, Ph.D.

Faculty Member: _____ Date: _____

Dr. Mohammad Mahinfalah, Ph.D.

Faculty Member: _____ Date: _____

Professor Gary Shimek, M.L.I.S.